ADVANCED FUNCTIONAL MATERIALS
www.afm-journal.de

# Wood-Derived Materials for Advanced Electrochemical Energy Storage Devices

*Jianlin Huang,* Bote Zhao, Ting Liu, Jirong Mou, Zhongjie Jiang, Jiang Liu, Hexing Li, and Meilin Liu**

**Over the past decade, wood-derived materials have attracted enormous interest for both fundamental research and practical applications in various functional devices. In addition to being renewable, environmentally benign, naturally abundant, and biodegradable, wood-derived materials have several unique advantages, including hierarchically porous structures, excellent mechanical flexibility and integrity, and tunable multifunctionality, making them ideally suited for efficient energy storage and conversion. In this article, the latest advances in the development of wood-derived materials are discussed for electrochemical energy storage systems and devices (e.g., supercapacitors and rechargeable batteries), highlighting their micro/nanostructures, strategies for tailoring the structures and morphologies, as well as their impact on electrochemical performance (energy and power density and long-term durability). Furthermore, the scientific and technical challenges, together with new directions of future research in this exciting field, are also outlined for electrochemical energy storage applications.**

## 1. Introduction

The rapid development of electrochemical energy storage (EES) devices (e.g., supercapacitors (SCs) and rechargeable batteries) as power sources for several emerging technologies (e.g., electric vehicles (EVs), smart grids, and portable electronic devices) have attracted tremendous attention in the past few decades because of their potential to offer high performance, long operational life, and good safety.[1] The development of novel electrode materials and design of electrode structure are critical to achieving high performance of these devices,[2] which have been considered as major challenges for the development of future EES technologies.[3] In addition to achieving high-performance, a few other challenges still remain, including reducing the cost, improving the safety, and addressing the environmental concerns of the next-generation green and sustainable EES devices.[4]

Recently, wood and its derivatives have attracted much interest from researchers as electrode materials for EES devices.[5] The wood-based materials have a hierarchically porous structure (such as vertical channels and numerous micro/nanopores) for fast transport of electrons and ions; they are also abundant, environmentally friendly, and renewable, making them ideally suited for EES device components, including electrodes, current collectors, separators, and template/substrate materials.[6] Carbonization of wood for advanced materials applications has been reported in the early 1990s.[7] Later on (in 2000s), the wood-derived carbon materials were further exploited to be used as electrode materials for EES by various modification/activation strategies.[8] Recently, wood and its derivatives were extensively studied in many fields with great success, especially in the development of nanotechnology.[5,6,9] The progress in the development of wood-based materials for EES with representative examples is briefly summarized in **Figure 1**.[79] It can be dated back to 1990s when the early study on physical properties of carbonized wood and its applications in making composites (e.g., carbon/polymer, carbon/carbon, and carbon/ceramic) was reported. Later on, wood-derived carbon materials were further used as electrodes for SCs and lithium-ion batteries (LIBs). Since 2013, the application of wood-derived materials was further extended to sodium-ion batteries (NIBs), and other batteries. Most recently, wood-based materials for EES have been boomed. In this respect, the Hu's, Berglund's, and Yu's groups have made great progress.[5,6,10,11,57] In comparison with conventional electrode materials, wood-based electrodes have unique advantages, such as hierarchically porous structure, superior mechanical performance, high electronic conductivity, and the potential to achieve high areal mass loading of active materials.

Prof. J. Huang, T. Liu, J. Mou, Prof. Z. Jiang, Prof. J. Liu
Guangzhou Key Laboratory for Surface Chemistry of Energy Materials
New Energy Institute
School of Environment and Energy
South China University of Technology
Guangzhou 510006, P. R. China
E-mail: jianlinhuang@scut.edu.cn
Dr. B. Zhao, Prof. M. Liu
School of Materials Science and Engineering
Georgia Institute of Technology
Atlanta, GA 30332-0245, USA
E-mail: meilin.liu@mse.gatech.edu
Prof. H. Li
The Education Ministry Key Lab of Resource Chemistry and Shanghai Key Laboratory of Rare Earth Functional Materials
Shanghai Normal University
Shanghai 200234, P. R. China
The ORCID identification number(s) for the author(s) of this article can be found under https://doi.org/10.1002/adfm.201902255.

**DOI: 10.1002/adfm.201902255**

Typical strategies for the use of wood in EES devices include 1) carbonizing wood directly as electrode active materials or current collectors; 2) using wood-derived carbon as a template to create electrodes preserving a multichanneled structure of pristine wood; 3) making wood-based electrode by coating conductive materials; and 4) using natural wood slice as separators.

To date, a few good reviews have summarized some recent advances in the development of wood-based materials for nanotechnologies and energy related applications.[5,6,10–12] However, a comprehensive review of wood-based materials in energy storage devices is still lacking. In this article, we summarize the latest progress in the development of wood-derived materials with structures designed and engineered for EES devices (as schematically shown in **Figure 2**), including LIBs, NIBs, Li–S batteries, Li–$O_2$ batteries, Li–$CO_2$ batteries, and SCs. A comprehensive discussion on the advantages and challenges of wood-derived materials is also presented. Further, we highlight some new directions in future research and offer future perspectives for next-generation energy storage and conversion devices based on wood-derived materials.

## 2. Structure and Properties of Wood

Wood is a porous and fibrous structural tissue, which could be found in the stems and roots of trees. The structure and component of wood have been widely discussed in the literatures.[5–12] As shown in **Figure 3**, wood has a typical hierarchically porous structure (including micro-, meso-, and macropores) and composition of multilayer cellulose (including cellulose, hemicellulose and lignin). The hierarchical structure of wood begins with millimeter scale of vessels and lumina, and continues with layered cell walls in micrometers. Wood cell walls are mainly composed of ≈40–50 wt% cellulose, ≈10–30 wt% hemicellulose, and ≈20–30 wt% lignin. These components interconnect with each other, ensuring a superior mechanical property of wood.[12] The hierarchical structure of cell wall continues with cellulose bundle in tens of nanometers, which can be further divided into elementary fibrils in 1.5–3.5 nm.[10] From molecular perspective, cellulose $(C_6H_{10}O_5)_n$ chain is composed of repeated units of glucose by hydrogen bonding and covalent bonding.[13]

Owing to their type and geographical difference, different woods show a wide variety of microstructures. Specifically, softwoods (e.g., pine, cedar, spruce, etc.) normally have a simple and homogeneous structure with a lot of fibers arranged in an ordered manner; they are more porous because of their fast growth rate. In contrast, hardwoods (such as balsa, basswood, oak, birch, and poplar) typically have a complex and heterogeneous structure, containing plentiful vessels and having higher density, denser porous structure, and stronger mechanical strength.[14] Although different woods have significantly different large-scale structures, there are similarities in their finer-scale porous structures. The structural anisotropy is an unique feature of woods, where many aligned vertical channels could be used as the rapid pathways for water, ions, and nutrients transport associated with photosynthesis.[15] Generally, there are two methods for the structure engineering of nanomaterials derived from woods: the bottom-up assembly based on nanocellulose and the top-down approaches that incorporate novel functionalities to natural wood with a hierarchically porous structure. Compared with the bottom-up approach, the top-down method is simpler, more efficient, and easier for scale-up application.[16]

With the advancement of nanotechnology, wood-derived nanomaterials have been widely used in many emerging areas, including environment, energy, and biomedicine.[5,6,12]

**Jianlin Huang** is an Associate Professor at the School of Environment and Energy at South China University of Technology. He received his Ph.D. degree from Shanghai Normal University in 2011. Prior to his current position, he worked as a postdoctoral fellow at McGill University, Canada, with Prof. Chao-Jun Li and Prof. Derek G. Gray. His research interests include the design and fabrication of novel nanomaterials for energy, environment, and biomass conversion technologies.

**Bote Zhao** is currently a postdoctoral fellow at the School of Materials Science and Engineering at Georgia Institute of Technology, USA. He received his B.S. and Ph.D. degrees from Nanjing Tech University, China. His research interests include the rational design, synthesis, and in situ/operando characterization of advanced materials for electrocatalysis, batteries, fuel cells, and supercapacitors.

**Meilin Liu** is a B. Mifflin Hood Chair, Regents' Professor, Associate Chair of Materials Science and Engineering, and codirector of the Center for Innovative Fuel Cell and Battery Technologies at Georgia Institute of Technology, USA. He received his B.S. degree from South China University of Technology and both his M.S. and Ph.D. degrees from University of California at Berkeley. His research interests include in situ/operando characterization and multiscale modeling of charge and mass transfer along surfaces, across interfaces, and in membranes, thin films and nanostructured electrodes to achieve rational design of materials and structures with unique functionalities for efficient energy storage and conversion.

 

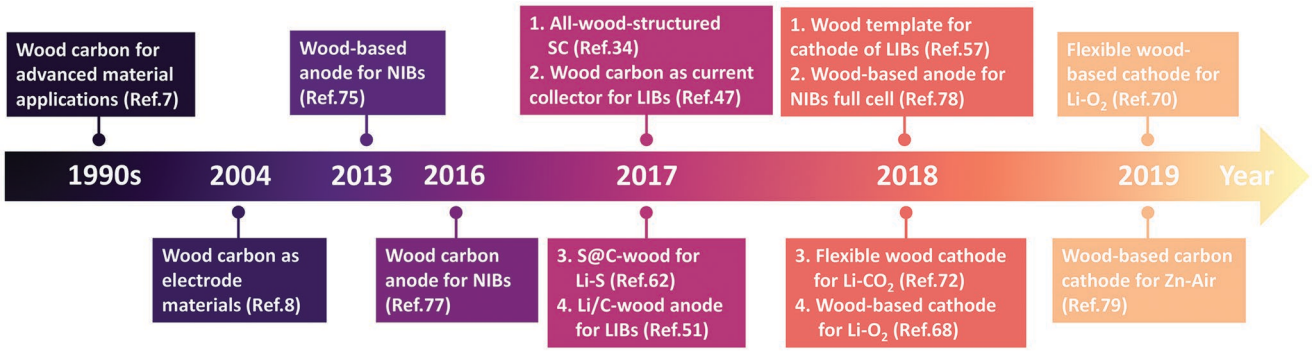


**Figure 1.** Progress in the development of wood-based materials for EES devices with representative examples.

In most cases, the selection of wood species for different applications is based on the physical and chemical properties of the wood, together with total wood procurement cost. Compared to softwoods, hardwoods (e.g., basswood, balsa, and poplar) generally show a wider application prospect in energy storage and conversion devices, benefiting from their relatively low density, high mechanical strength, and denser porous structure.[14] However, there is no absolutely standard for selection of wood species for different applications, because it still depends on specific uses and treatment methods of wood.[29]

It can be expected that wood will show many unique properties based on functionalization treatment by nanotechnologies. In this section, recent advance in designing and synthesizing wood-based nanomaterials with hierarchical structures and novel properties has been summarized.

### 2.1. Novel Properties of Wood-Based Materials

In recently years, wood-based materials with some novel properties based on functional modification/treatment have been developed, such as transparent wood,[15] functionalized transparent wood,[18] plasmonic wood,[22] flexible wood,[26] superstrong wood,[29] and wood-based carbon sponge and aerogels.[33]

#### *2.1.1. Transparent Wood and Functionalized Transparent Wood*

Transparent wood was fabricated by removing the light-absorbing materials in wood and followed by permeating refractive index (e.g., epoxy resin) into wood (**Figure 4**a), showing clearly transparency for a sample with 3 mm thickness (Figure 4b).[15] Similarly, the compound (methyl methacrylate) was introduced into wood by in situ polymerization

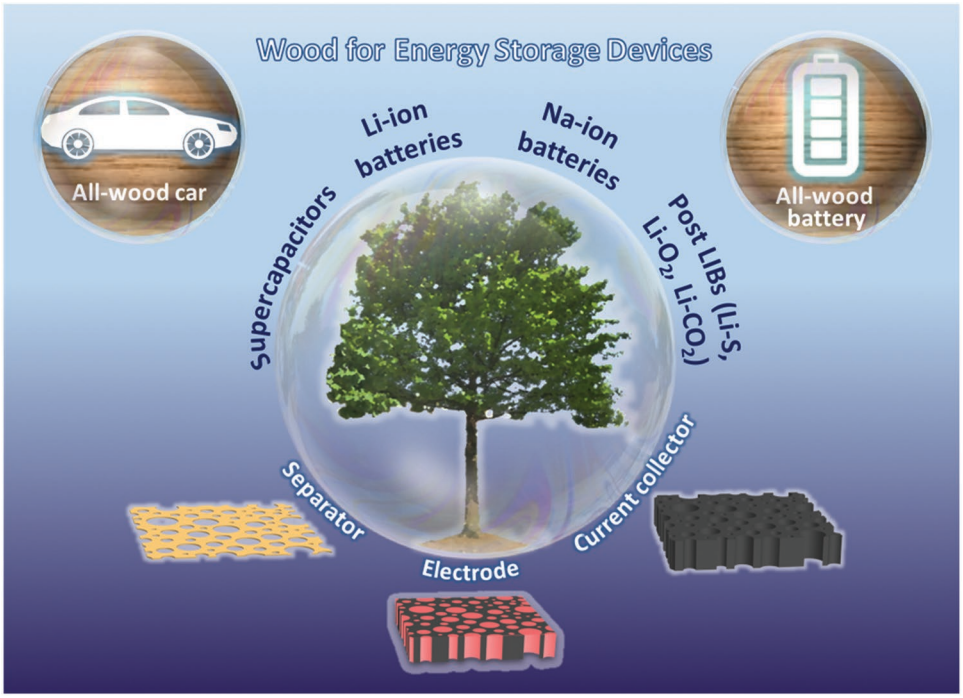


**Figure 2.** Schematic illustration of the main topics in this review, including wood resources, wood-derived materials fabrication, and structural and functional design for the EES devices (including SCs, LIBs, NIBs, and other batteries).

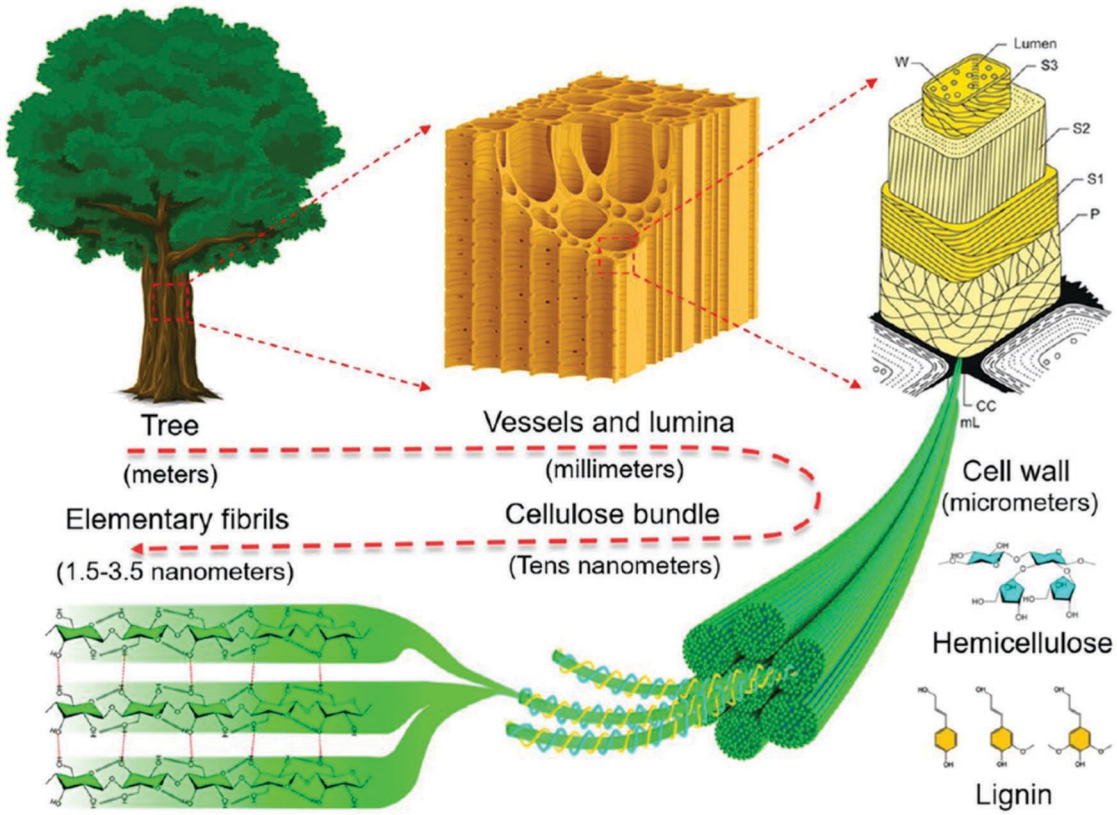


**Figure 3.** Graphical illustration of the hierarchical structure of wood, and the composition of cell wall. Reproduced with permission.[6] Copyright 2018, American Chemical Society.

method to make transparent wood.[17] The light transmittance of the transparent wood decreased with gradually increasing the thickness. This work suggests that the toughness, strength and transparency of wood can significantly be increased with forming a polymer-based composite.

Functional transparent wood has also been developed.[10] For example, luminescent transparent wood was prepared by incorporating Si and CdSe/ZnS core/shell quantum dots (QDs), and the luminescence diffusivity could be controllable by the light scattering of transparent wood (Figure 4c,d).[18] Meanwhile, the fluorescent dye rhodamine 6G and poly(methyl methacrylate) (PMMA) were also infiltrated into transparent wood, leading to a broader laser emission from the transparent wood based on aligned cellulose fibers as optical resonators (Figure 4e).[19] In addition, the magnetic transparent wood has also been fabricated by modified wood with ferromagnetic materials.[20] Yu et al. showed a transparent wood with controllable thermal energy by adding near-infrared radiation absorbing $Cs_xWO_3$ nanoparticles, resulting in a high transparency of 86% at 550 nm for visible light transmittance, and high near-infrared absorption from 780 to 2500 nm for heat shielding.[21]

### 2.1.2. Plasmonic Wood

To further expand wood applications, the metallic nanoparticles (NPs) with plasmonic properties are used to modify wood. Plasmonic wood has been successfully fabricated by deposition of metal nanoparticles (e.g., Pd, Au, and Ag NPs) within wood micro/mesostructures.[22] The plasmonic wood coated with Pd NPs could convert the incident light into heat energy due to the plasmonic effect (Figure 4g,h). Moreover, the heat limited on the micro/nanochannel surface of wood, resulting in a high effectively solar steam generation.[23] Additionally, the plasmonic wood with good hydrophobicity could be effective for water transport, keeping a continuous water supply for the vapor generation (Figure 4i). Such a plasmonic wood, with an integral structure, is different from the separated bilayer structure of the wood–GO evaporator.[24] In addition, a wood slice modified with $CuFeSe_2$ NPs has also been developed for highly efficient solar steam generation and water purification.[25]

### 2.1.3. Flexible Wood

Flexible wood would be very unique with the promising potential application in flexible personal devices. However, fabrication of flexible wood is challenging due to the fact that wood is usually a bulk with stiffness nature. Recently, a simple and scalable top-down method has been developed for fabricating superflexible wood,[26] which is totally different with original wood due to the change of chemical and physical properties (Figure 4k). The obtained flexible wood slice was used as a bioscaffold to attach the HEK293 cells for testing cell attachment and biocompatibility.

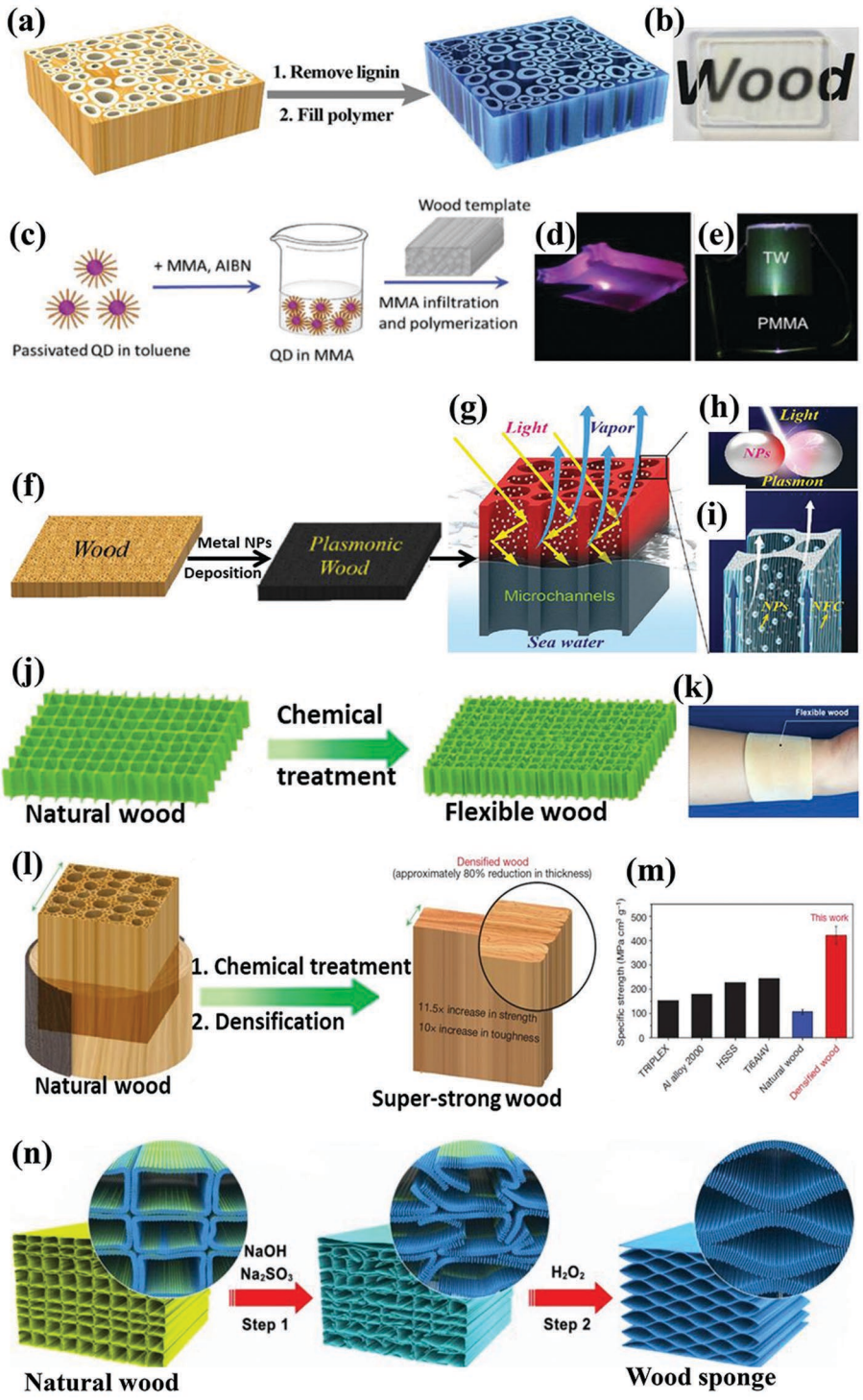


**Figure 4.** a) Schematic to show the fabrication of transparent wood; b) a photograph of the transparent wood. a,b) Reproduced with permission.[15] Copyright 2016, Wiley-VCH. c) Schematic and photograph of quantum dot luminescent transparent wood. d) Photograph of Si QD transparent wood under 405 nm laser pumping. e) Photograph of CdSe QD transparent wood integrated in a larger PMMA piece. c–e) Reproduced with permission.[18] Copyright 2017, Wiley-VCH. f) Schematic to show the fabrication of plasmonic wood; g) after metal nanoparticle decoration, light can be guided into the wood lumen and be fully absorbed for steam generation. h) Schematic of plasmonic effect of two adjacent metal NPs. i) Zoomed-in schematic illustrating the water transport along microchannels in wood. f–i) Reproduced with permission.[22] Copyright 2017, Wiley-VCH. j) Schematic illustration of treatment process for superflexible wood; k) a photoimage of flexible wood membrane. j,k) Reproduced with permission.[26] Copyright 2018, American Chemical Society. l) Schematic of the top-down, two-step approach to transforming bulk natural wood directly into superstrong densified wood; m) specific tensile strength of the resulting densified wood. l,m) Reproduced with permission.[29] Copyright 2018, Springer Nature. n) Graphical illustration of the chemicals and structure evolutions of natural balsa wood upon chemical treatment. Reproduced with permission.[31] Copyright 2018, Elsevier.

This work suggests that the flexible wood can successfully be prepared via a simple chemical treatment method directly from natural wood, and resulting in the flexible wood used as an efficient bioscaffold material.

#### 2.1.4. Superstrong Wood

In general, designing a material with high strength and toughness simultaneously is an insurmountable challenge.[27,28] Very recently, a prominent attempt to achieve this challenging goal was reported.[29] A simple but effective strategy has been proposed to prepare a densified wood with an ultrahigh mechanical property directly from original wood. The preparation process involves two steps, that is, the partial removal of lignin and hemicellulose from the natural wood and followed by hot pressing, leading to a completely densified wood (Figure 4i). The as-made densified wood showed outstanding mechanical properties, which surpassed most of widely used structural materials including plastics, steel and alloys. This work suggests that the superstrong wood with ultrahigh strength and toughness can be achieved simultaneously by partial removal of lignin and hemicellulose and followed by hot-pressing treatment.

#### 2.1.5. Wood-Derived Carbon Sponge and Aerogels

Lightweight and compressible carbon materials with high conductivity, large surface area, and high porosity have aroused extensive interests due to their wide applications such as catalysis, water treatment, energy storage, and sensors.[30] Recently, a highly compressible and anisotropic lamellar wood carbon sponge (WCS) has been successfully prepared directly from natural wood via chemical treatment followed by carbonization.[31] As graphically illustrated in Figure 4n, the lignin, hemicellulose and partial cellulose could be removed by using $S_2O_3$ ions as nucleophilic reagents. Meanwhile, the thin cell walls generated many pores, and even broken with continuous reaction processing. Further reaction with $H_2O_2$ continuously removed lignin and hemicellulose, leading to complete breakage of the thin cell walls. These broken thin cell walls were attached to the nearest unbroken cellulose fibers during freeze drying, resulting in a porous, interconnecting, lamellar structural material. With further carbonization treatment, the unique lamellar structure can be well preserved.

Due to the high porosity between each layer in the unique lamellar multiarched structure, the WCS is particularly lightweight with a density of 15 mg $cm^{-3}$, which is 3.5 times lower than the other delignified wood and much lower than the natural wood. In addition, the WCS material has a promising potential for high-performance strain sensors based on its superior mechanical compressibility, and excellent pressure sensitivity. However, the WCS-based strain sensor cannot detect very weak movements like human pulses, which suggests that it is absolutely necessary to further improve performance of the WCS material in future.

Besides the WCS, wood-derived aerogels have also been developed by a catalytic pyrolysis method.[32] The synthesis process of the wood-derived carbon nanofiber (CNF) aerogel is carried out as following steps. First, the nanofiber cellulose (NFC) suspension was synthesized by a common oxidation of wood pulp with 2,2,6,6-tetramethylpiperidine-1-oxyl (TEMPO). Second, the wood–NFC hydrogel was converted to the wood–NFC aerogel by $CO_2$ critical-point drying. Finally, the pyrolysis of the Wood–NFC aerogels was performed under inert gas at a high temperature of ≈900 °C to produce the final wood derived CNFs aerogels. The as-obtained CNFs aerogels had a 3D nanofibrous frameworks, and exhibited a superior electronic conductivity and high specific surface area. These properties endow CNFs aerogels a promising potential as self-standing electrodes of SCs.

Above all, the structural features of wood include structural anisotropy, aligned channels, and hierarchically porous structure combining micro-, meso-, and macropores.[5,10] In wood cell walls, lumens are of micrometer scale, and normally of cylinder shape, aligned in a particular direction. Pits usually include micro- and mesopores. Hierarchical pores can be scattering light due to gas/solid interface boundaries, and thus hindering light transmittance.[15] Based on structural features of wood, the wood-based materials have unique advantages for energy storage compared to traditional electrodes, including its large thickness and high mass loading, straight channels with low tortuosity, and plentiful pathways for the fast transport of electrons and ions, in addition to being an abundant and renewable resource.[6,35] Additionally, different from the traditional bottom-up approach, the fabrication of wood-based electrode usually involves top-down processes, which allows the intrinsic unique structure of wood, featuring multiple aligned channels (e.g., luminas and vessels), to be well preserved.[16] Moreover, these advantages of wood structure for energy storage can be fully utilized by a top-down approach. Wood structures are naturally rich in aligned channels with strong mechanical strength that can be well retained after post treatment and even high-temperature carbonization, while endowing the wood carbon (WC) with high electrical conductivity.[34,35] These structural characteristics, along with the facile fabrication, make wood and its derivatives ideal electrode materials (especially for thick electrode design) in energy storage devices.

Detailed application in energy storage devices for the functional wood carbon will be discussed in the following sections.

## 3. Wood-Derived Materials in Supercapacitors

SCs represent one of the most attractive EES devices for a diverse range of applications that require rapid power delivery and recharging.[33] According to different charge storage mechanisms, SCs can be classified into two types of capacitors, those are, electrical double layer capacitors (EDLCs), and pseudocapacitors. The charge storage of EDLCs depends on electrostatically adsorption of electrolyte ions on the active electrode materials surface, while, pseudocapacitors depend on reversible faradaic reactions to store energy. Carbon materials (e.g., activated carbon, carbon nanotubes (CNTs), graphene, and carbon nanofibers) with high conductivity and large specific surface area are usually used as electrode materials for the EDLCs. The

electrodes used for pseudocapacitors are usually metal oxides, conductive polymer and so on, which could deliver much higher theoretical capacitance compared to the carbon-based materials.

Wood-derived micro/nanomaterials as electrodes of SCs have recently achieved significant progress.[34,35] Carbonized wood (CW) is an ideal candidate for construction of high-performance electrodes. We can use CW directly as a self-standing and binder-free electrode without additional conductive agents and current collectors. Moreover, CW has intrinsic properties of high ionic/electronic conductivity, light weight, and open vertical channels. In this section, the applications of wood and its derived materials in electrochemical SCs will be highlighted.

### 3.1. Carbonized Wood as Electrodes

Wood in general needs to be carbonized/or activated before using as an electrode material.[36a,b] **Figure 5** shows common synthesis methods of carbonization/activation for natural wood, including inert or air atmosphere carbonization, hydrothermal carbonization, and chemical reagent activation/carbonization. Although the high temperature (typically at ≈900 °C) carbonization in inert gas atmosphere is considered to be a relatively simple yet efficient route, the obtained CW usually displays a poor electrochemical performance. Therefore, the surface modification of carbonized wood is necessary to further improve the specific capacitance of SCs. For example, a porous wood carbon monolith (m-WCM) was reported through carbonization of poplar wood followed by surface modification using a $HNO_3$ solution.[36c] In comparison with WCM, the specific surface area of m-WCM decreased from 467 to 416 $m^2\ g^{-1}$ after surface modification, which suggests that the oxygen-containing functional groups of −COOH, −OH, and $-NO_2$ are successfully introduced on m-WCM surface, leading to an increase of the specific capacitance. The as-made m-WCM could be directly used as a freestanding electrode for SCs, which delivered a maximum gravimetric capacitance of 234 F $g^{-1}$ at 5 mA $cm^{-2}$ in a 2 M KOH solution. After 2000 cycles at 10 mA $cm^{-2}$, the m-WCM showed a good stability with a capacitance retention over 97%. Similarly, a biochar wood-based active carbon (AC) was synthesized through a simple activation of biochar wood

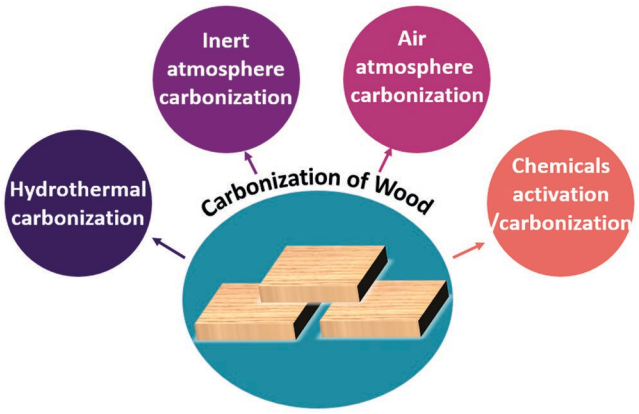


**Figure 5.** The carbonization/activation route of natural wood.

with a diluted $HNO_3$ solution at room temperature, which delivers 7 times higher specific capacitance (115 F $g^{-1}$).[37]

Hydrothermal synthesis is another widely used to synthesize various carbonaceous materials for SCs, due to the low-cost, and mild temperature. For example, Wei et al. demonstrated that the active wood (AC-W700 and AC-W800) with large specific surface area and highly open pores could be synthesized by hydrothermal carbonization method.[38] **Figure 6**a shows an irregular morphology of the resulting activated carbon particles (AC-W700 and AC-W800) with a diameter of 1–20 µm. As shown in Figure 6b,c, the specific capacitance of AC-W800 electrode was more than 236 F $g^{-1}$ (100 F $cm^{-3}$) at a scan rate of 1 mV $s^{-1}$, which is higher than that of AC-W700 and commercial activated carbons for EDLCs performance. Moreover, the energy density of commercial devices using AC-W800 as electrode was two times than those activated carbons made by conventional method.

In addition, Tang et al. used a basswood slice to prepare a low-tortuosity, multichannel, mesoporous carbon frameworks.[39] Both porous fabrication and surface functionalization are achieved simultaneously by heteroatoms doping and subsequent $NH_3$ activation. Scanning electron microscopy (SEM) image indicated the anisotropic, and multichannels are preserved during the pyrolysis process (Figure 6d). The specific capacitance of N,S-codoped wood carbon (TARC-N) was up to 704 F $g^{-1}$ at 0.2 A $g^{-1}$, which was more than two times that of TARC (290 F $g^{-1}$) and four times than that of RC (169 F $g^{-1}$). As shown in Figure 6e,f, the supercapacitor of TARC-N maintained a capacitance retention of 94% after 5000 cycles at 2 A $g^{-1}$. Moreover, the TARC-N was investigated as a cathode catalyst for Zn–air batteries. The Zn–air battery showed an open circuit voltage of ≈1.47 V and a maximum power density of 241 mW $cm^{-2}$, as well as a high energy density of 945.2 Wh $kg^{-1}$ at 10 mA $cm^{-2}$. Therefore, both the porosity and the heteroatoms doping of electrode materials will facilitate to improve SCs performance. Recently, we reported an active carbonized wood (ACW) via facile a one-pot activation of natural wood at 450 °C for 2 h in air atmosphere. The as-prepared ACW exhibited an excellent specific capacitance of ≈6.85 F $cm^{-2}$ (≈235 F $g^{-1}$) at the current density of 1.0 mA $cm^{-2}$, as a freestanding electrode of SCs (Figure 6g–i). The specific capacitance of the ACW electrode is much higher than those carbonization at high temperature (≈900 °C) in an inert atmosphere and commercial active carbon materials.[34,35] The superior electrochemical performances of the ACW electrode can be ascribed to the hierarchically porous, 3D structure, and some oxygen-containing functional groups of the ACW surface, which together contribute to performances of the EDLCs and pseudocapacitance. In addition, some representative wood-based materials to fabricating supercapacitors are summarized in **Table 1**.

### 3.2. Wood-Derived Electrodes

CW with hierarchically porous framework feature is also an ideal 3D conductive substrate/scaffold for growth of active electrode materials, such as metal oxides/hydroxides, conductive polymer with high theoretical capacitance.[40] The hierarchically

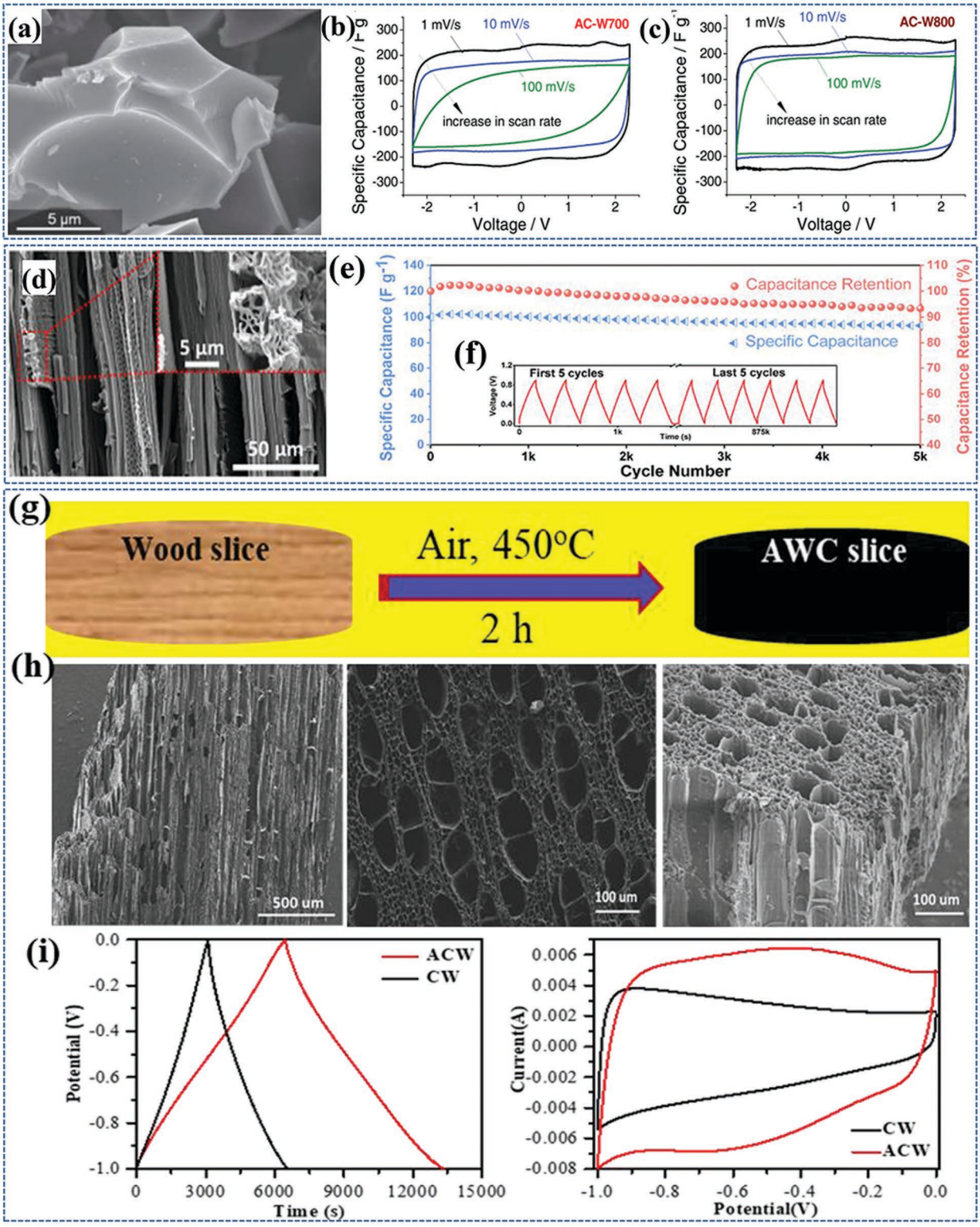


**Figure 6.** a) SEM images for TARC-N: cross-sectional view. Insets show high-magnification SEM images; b) cycling stability for 5000 cycles at a current density of 2 A $g^{-1}$, and c) the inset shows the charge/discharge profiles obtained from first and last 5 cycles. a–c) Reproduced with permission.[38] Copyright 2011, Wiley-VCH. Morphology and chemical performance of the carbon materials obtained by hydrothermal carbonization: d) SEM image showing typical particle morphology; e,f) cyclic voltammograms (CV) of the carbon samples. d–f) Reproduced with permission.[39] Copyright 2018, Elsevier. Active carbonized wood obtained by carbonization in an air atmosphere: g) graphical illustration for the fabrication process of ACW; h) SEM images for ACW; i) galvanostatic charge/discharge and CV for ACW and CW electrodes. g–i) Unpublished data.

**Table 1.** Summary of some parameters of various wood-based materials for SCs.

| Wood species | Carbonization condition [°C] | Activation condition | Surface area [$m^2 g^{-1}$] | Active mass loading | Electrochemical performance | Electrolyte | Cycles [%] | Ref. |
|---|---|---|---|---|---|---|---|---|
| Fir wood | 900/$N_2$ | – | 1131 | – | 142 F $g^{-1}$ at 25 mV $s^{-1}$ | 0.5 M $HNO_3$ | – | [8a] |
| Fir wood | 780/$N_2$ | KOH | 1064 | – | 180 F $g^{-1}$ at 10 mV $s^{-1}$ | 0.5 M $H_2SO_4$ | – | [8b] |
| Poplar wood | 900/$N_2$ | $HNO_3$ | 416 | – | 234 F $g^{-1}$ at 5 mA $cm^{-2}$ | 2 M KOH | 2000/≈97% | [36c] |
| Eucalyptus wood | 250/Hydrothermal | 800/$N_2$ | 2387 | – | 236 F $g^{-1}$ at 1 mV $s^{-1}$; 175 F $g^{-1}$ at 20 A $g^{-1}$ | $TEABF_4$/AN | – | [38] |
| Red cedar wood | 750/$N_2$ | $HNO_3$ | 400 | – | 115 F $g^{-1}$ at 3 A $g^{-1}$ | 0.5 M $H_2SO_4$ | 5000 | [37] |
| Beech wood<br>Pine wood<br>Sandal wood | 800/$N_2$ | – | 44<br>76<br>38 | – | 39.2 Wh $kg^{-1}$ at 200 mA $g^{-1}$<br>45.6 Wh $kg^{-1}$ at 200 mA $g^{-1}$<br>32.9 Wh $kg^{-1}$ at 4000 mA $g^{-1}$ | 2 M KOH | 2000/99.7% | [36a] |
| Eucalyptus wood | 900/$N_2$ | $CO_2$ | 921 | – | 260 F $g^{-1}$ at 5 mA $cm^{-2}$<br>36 Wh $kg^{-1}$ (12 Wh $L^{-1}$)<br>2181 W $kg^{-1}$ (78 W $L^{-1}$) | 2 M $H_2SO_4$ | – | [36b] |
| Basswood | 950/$N_2$ | $NH_3$ | 1438 | – | 135 F $g^{-1}$ at 0.2 A $g^{-1}$<br>15.2 Wh $kg^{-1}$ at 0.2 A $g^{-1}$<br>8.9 Wh $kg^{-1}$ at 3234 W $kg^{-1}$ | 4 M KOH | 5000/94% | [39] |
| Beech wood; $MnO_2$/C | 850–1600/$N_2$ | – | – | 3 wt% | 592 F $g^{-1}$ at 1 mV $s^{-1}$ | 1 M $Na_2SO_4$ | 1000/100% | [41] |
| Basswood<br>CW-FeOOH-PEDOT | 900/Ar | – | 235 | 50 mg $cm^{-3}$ | 126 F $g^{-1}$ at 10 m A $cm^{-2}$<br>114.6 F $cm^{-3}$ at 50 mg $cm^{-2}$ | 2 M KOH | 5000/85% | [40e] |
| Basswood blocks<br>$MnO_2$@WC | 1000/Ar | $CO_2$ | – | 75 mg $cm^{-2}$ | 3.6 F $cm^{-2}$ 1.6 mW $cm^{-2}$<br>at 1044 mW $cm^{-2}$ | 1 M $Na_2SO_4$ | 10 000/93% | [34] |
| Poplar wood; $Co(OH)_2$/CW | 1000/$N_2$ | – | 568 | 5.7 mg $cm^{-2}$ | 3.723 F $cm^{-2}$ (648.6 F $g^{-1}$)<br>at 1.0 mA $cm^{-2}$<br>0.69 mWh $cm^{-2}$ (10.87 Wh $kg^{-1}$)<br>at 1.126 W $cm^{-2}$ (17.75 W $kg^{-1}$) | 2 M KOH | 10 000/85% | [35] |

porous structure is favorable for the contact between electrode and electrolyte. The straight channels of CW facilitate ion transport and provide a large specific surface to achieve high loading of active materials.

For example, Gutierrez-Pardo et al. reported a 3D porous and conductive carbon scaffold via pyrolysis of beech wood for the direct growth of $MnO_2$ nanosheets. The resulting hybrid material ($MnO_2$/C) was used as a binder-free electrode for SCs applications.[41] The $MnO_2$/C electrode exhibited a capacitance of 592 F $g^{-1}$ and an excellent cyclic stability, which was attributed to the micro/nanostructure of the CW and a higher crystallinity of $MnO_2$. To meet the increasing demands for the energy storage devices with a higher energy/power density, lower cost, longer cycle life and environmental friendliness. An all wood–structured asymmetric supercapacitor (ASC) was developed based on an activated wood carbon (AWC) anode, a $MnO_2$/wood carbon ($MnO_2$@WC) cathode, and a wood membrane separator (**Figure 7**a).[34] The large thickness (≈1 mm) of the AWC can achieve a high areal mass loading (>75 mg $cm^{-2}$), which is the highest loading of the $MnO_2$-based supercapacitor among all ever-reported. As a result, the all wood–structured ASC exhibited a high areal capacitance (3.6 F $cm^{-2}$), high energy density of 1.6 mW $cm^{-2}$ at 1044 mW $cm^{-2}$ and a long cycling life (Figure 7b–d), which is attributed to the unique structural advantages including multichannels, low tortuosity, high mass loading (75 mg $cm^{-2}$), as well as high ionic and electronic conductivity.

Inspired by previous works,[22,32,34] most recently, we developed and expanded the potential of wood-based energy storage materials and devices by combining a porous wood framework with high-capacity active electrode materials such as $Co(OH)_2$, $Ni(OH)_2$, and $Fe_2O_3$ to construct high-performance ASC.[35] Figure 7e shows the synthesis process of a wood-derived all-solid-state ASC. As shown in Figure 7f,g,m–o, after the homogeneous growth of $Co(OH)_2$ nanoflakes on outer and inner surface of the CW, a thicker channel wall and smaller channel diameter could be achieved. Besides, the energy-dispersive X-ray spectroscopy (EDS) (Figure 7p–r) further confirmed uniform distribution of C, O, and Co elements in $Co(OH)_2$@CW. The $Co(OH)_2$@CW electrode showed an outstanding rate capability (3.723 F $cm^{-2}$, and 1.568 F $cm^{-2}$, at 1.0 and 30 mA $cm^{-2}$ respectively) (Figure 7s,t), which is much better than most of $Co(OH)_2$-based electrodes of supercapacitance. In addition, the wood-derived ASC delivered an energy density of 0.69 mWh $cm^{-2}$ (10.87 Wh $kg^{-1}$) at a power density of 1.126 W $cm^{-2}$ (17.75 W $kg^{-1}$), as well as a long cycling performance over 10 000 cycles at 1.0 A $g^{-1}$ (Figure 7i–l). The unique hierarchically porous carbon frameworks are believed to be the major favorable advantage to achieve high energy/power densities due to full exposure of active electrode materials, fast ions transport and efficient current collection. This work demonstrates a thick electrode design directly using carbonized wood as current collector and electrode material (Figure 7h), which indicates both high capacity and energy density, especially based on device level.

Additionally, with an increasing demand for flexible energy storage devices, the paper-based electrodes derived from

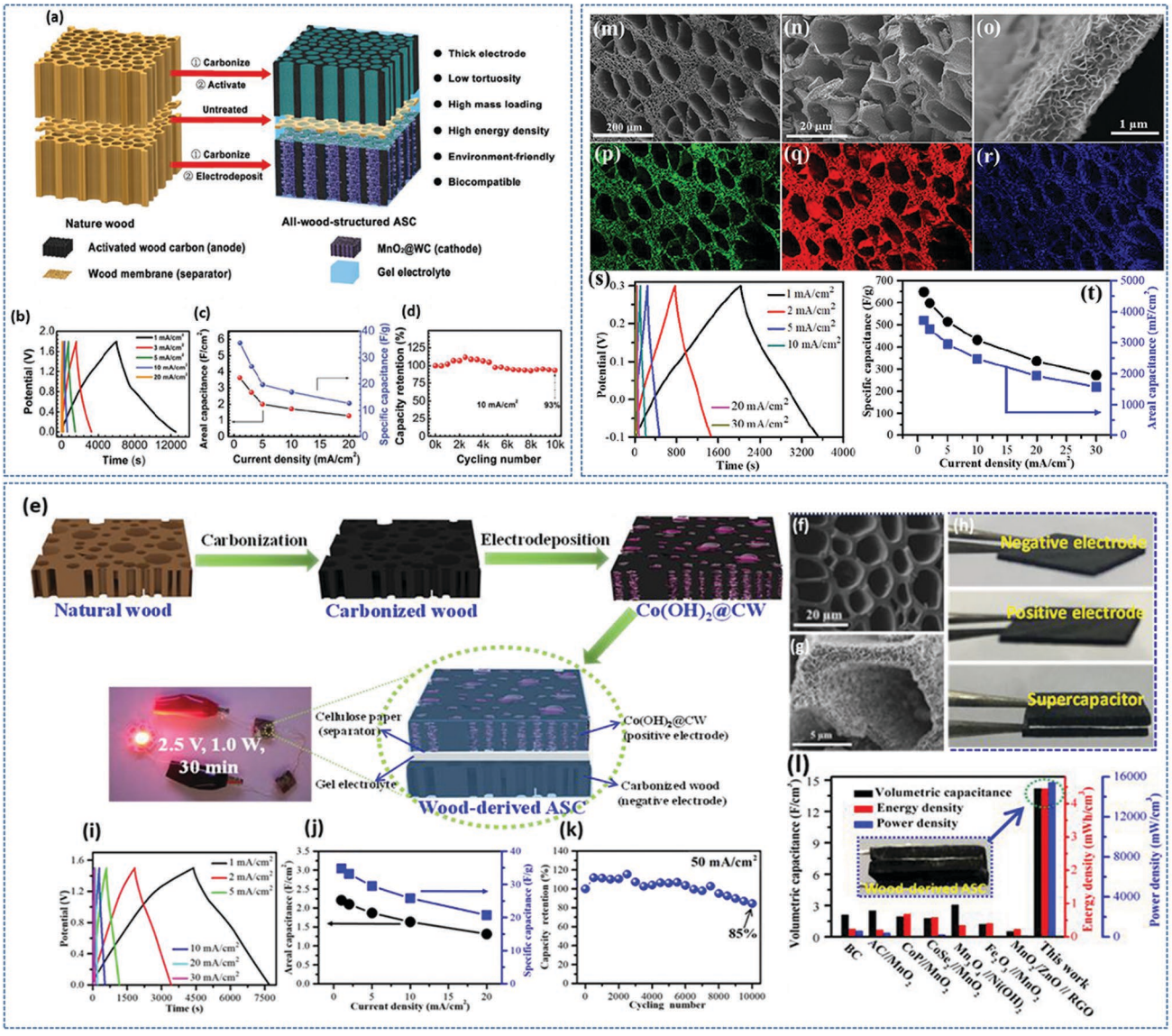


**Figure 7.** a) Graphical illustration of construction process for the all-wood structured supercapacitor. Electrochemical performance of the AWC//wood separator//$MnO_2$@WC ASC: b) charge–discharge profiles at different current densities; c) rate performances and d) cycling performance. a–d) Reproduced with permission.[34] Copyright 2017, Royal Society of Chemistry. e) Fabrication of a wood-derived all-solid-state asymmetric supercapacitor based on a carbonized wood as negative electrode, a cellulose paper as separator, and a $Co(OH)_2$@CW as positive electrode in a sandwich-like structure. SEM images of CW f) and $Co(OH)_2$@CW g,m–o), and photograph of electrodes and all-sold-state ASC h). Electrochemical performance of CW/PVA-KOH/$Co(OH)_2$@CW ASC: i) charge–discharge profiles at different current densities, j) rate performances based on the GCD curves at different current density, k) the ASC device measured at 50 mA $cm^{-2}$ for 10 000 cycles, and l) energy/power density and volumetric capacitance of the wood-derived ASC compared with the previously reported electrode materials. Elemental mapping images of p) C, q) O, and r) Co, respectively, in (m). Electrochemical performance of the $Co(OH)_2$@CW electrode: s) charge–discharge profiles at different current densities and t) rate performances. e–t) Reproduced with permission.[35] Copyright 2018, Wiley-VCH.

cellulose-based natural wood material hold great promise for such applications due to its low cost, abundance, renewable, and sustainable properties.[42,43] Edberg et al. reported an all-organic paper SCs based on CNF, and the conductive polymer PEDOT:PSS.[44] The specific capacitance of the composite electrode increased to 230 from 110 F $g^{-1}$ and the areal capacitance from 160 mF $cm^{-2}$ to 1 F $cm^{-2}$ due to the introduction of sulfonated lignin. Furthermore, the supercapacitor showed a long cycling stability after 700 charge/discharge cycles without significant performance degradation, through introducing lignosulfonate into the electrolyte solution. Recently, Yu's group[32] reported ultrathin carbon nanofiber aerogels with a diameter of 6 nm derived from wood–NFC (nanofiber carbon) via a catalytic pyrolysis method. The carbon nanofiber aerogels showed a high electrical conductivity of 710 S $m^{-1}$ and large specific surface area of 553–689 $m^2$ $g^{-1}$. The capacitance of the carbon nanofiber aerogels was more than two times than that of pure Wood–NFC, which was attributed to the introduction

**Table 2.** Summary of some parameters of various wood-based materials for LIBs.

| Wood species | Carbonization condition [°C] | Function | Electrochemical performance | Ref. |
|---|---|---|---|---|
| Mangrove charcoal | 1000/Ar | Derived carbon as anode | 335 mAh $g^{-1}$ (under 0.5 V), ICE = 73.7%. | [48] |
| Mangrove green tree | 500/Ar | Derived carbon as anode | 424 mAh $g^{-1}$ at 30 mA $g^{-1}$, ICE = 81% | [49] |
| Loblolly pine trees | 850 °C/$N_2$ | Derived carbon as anode | 1000 mAh $g^{-1}$ at 50 °C, at 0.1 C | [50] |
| Basswood | 1000/Ar | Li-metal/carbonized wood as anode | 2650 mAh $g^{-1}$ (75 mAh $cm^{-2}$), ≈150 h at 3 mA $cm^{-2}$ | [51] |
| Wood fiber | 600 °C/$N_2$ | MnO/wood fiber as anode | 952 mAh $g^{-1}$ at 0.1 A $g^{-1}$, 100 cycles | [52] |
| Softwood pulp derived NFC | 1000/95% Ar:5%$H_2$ | Carbonized c(GO + NFC) fibers as anode | 312 mAh $g^{-1}$, at 25 mA $g^{-1}$, 63 cycles | [53] |
| Basswood blocks | 1000/Ar | Derived carbon as current collector | 7.6 mAh $cm^{-2}$ (95 Ah $L^{-1}$) | [47] |
| Pine wood | 800/Air | As a biotemplate for LNMO cathode | 124 mAh $g^{-1}$ at 2 C, 97 mAh $g^{-1}$ at 10 C, retention of 90% after 100 cycles | [55] |
| Pinewood blocks | 700/Air | As a template for LCO cathode | 22.7 mAh $cm^{-2}$ | [57] |

of TsOH, leading to decreasing the stacked structure and maintaining the 3D nanofibrous network of carbon aerogels. The carbon nanofiber aerogels displayed a specific capacitance of 140 F $g^{-1}$ at 0.5 A $g^{-1}$ as a binder-free electrode for SCs.

Although exciting breakthrough in improving the specific capacitance and energy density has been made, there are still some key problems for the practical application of SCs based on wood-derived materials. For example, new modification and treatment methods are yet to be developed for improving the electrical conductivity and mechanical properties (e.g., strength, toughness, and flexibility) of wood-based materials toward high-performance SCs electrodes. Additionally, more attention should be given to enhance the electrochemical performance of full device for practical application. The design of thick electrode with high mass loading is another promising direction to further improve the energy density of device.

## 4. Wood-Derived Materials in LIBs

Rechargeable LIBs have been applied widely in electronic devices such as EV and hybrid EV (HEV) due to their high energy density, high safety, and long cycling life.[45,46] A typical LIBs configuration contains cathode, anode, electronic insulative separator, and $Li^+$-conducting electrolyte. For conventional electrode preparation for LIBs, the active electrode materials are mixed with binder and conductive additive together in an organic solvent to form slurry, and the slurry is then casted onto metallic current collectors (e.g., Al or Cu foil) to form an electrode. However, there are still several technical constraints on LIBs performance: 1) the additives and current collectors do not contribute to capacity, which decrease the specific energy density; 2) weak mechanical stability leads to low packing density and the detachment of electroactive material from the current collector. Moreover, with the increase of environmental consciousness, sustainability and eco-friendliness should be taken into account for developing future energy storage devices.[47] Therefore, development of wood and its derivative materials is a promising alternative to LIBs, due to the unique structure, environmental friendliness, and sustainability.

In this section, we discuss the recent progress in wood and its derivative materials for LIBs, mainly focusing on the multipurpose as electrode material, current collector, separator, and template/substrate.

### 4.1. Wood-Derived Materials for Anode Materials

The natural wood possesses hierarchical structures, strong mechanical robustness, and exhibits high electrical conductivity after high temperature carbonization under inert atmosphere. These features of wood-based materials can significantly promote the fast transport of ions and electronics, making wood-derived carbon as a desirable electrode material or template for LIBs (**Table 2**).

In 2010, Liu et al. studied the mangrove charcoal–derived hard carbon (MC) as an anode for LIBs.[48] MC carbonized at 1000 °C delivered the highest discharge specific capacity of 335 mAh $g^{-1}$, first-cycle Coulombic efficiency (CE) of 73.7%, good rate performance and cycling stability. To increase initial CE, Yoon's group investigated the effects of heat pretreatment temperature (450–600 °C) on MC.[49] After heat pretreatment, the hard carbon, with a higher synthetic yield of 30 wt%, achieved enhanced initial CE of 81% compared to that obtained by a one-step carbonization, which was attributed to the low H/C and $O_{diff}$/C ratios and a porous structure promoting lithium-ion insertion/extraction. This work confirms that the wood-derived carbon materials can be acted as an ideal anode for high-performance LIBs. Moreover, Adams et al. utilized the loblolly pine woodchip-derived carbon to construct porous electrode of LIBs via an industrial KOH activation and pyrolysis process.[50] The produced porous carbon showed micro/mesoporosities and high special surface area (1580 $m^2$ $g^{-1}$), enabling improvement of $Li^+$-storage capacity. Furthermore, the woodchip-derived porous carbon electrode showed a stable

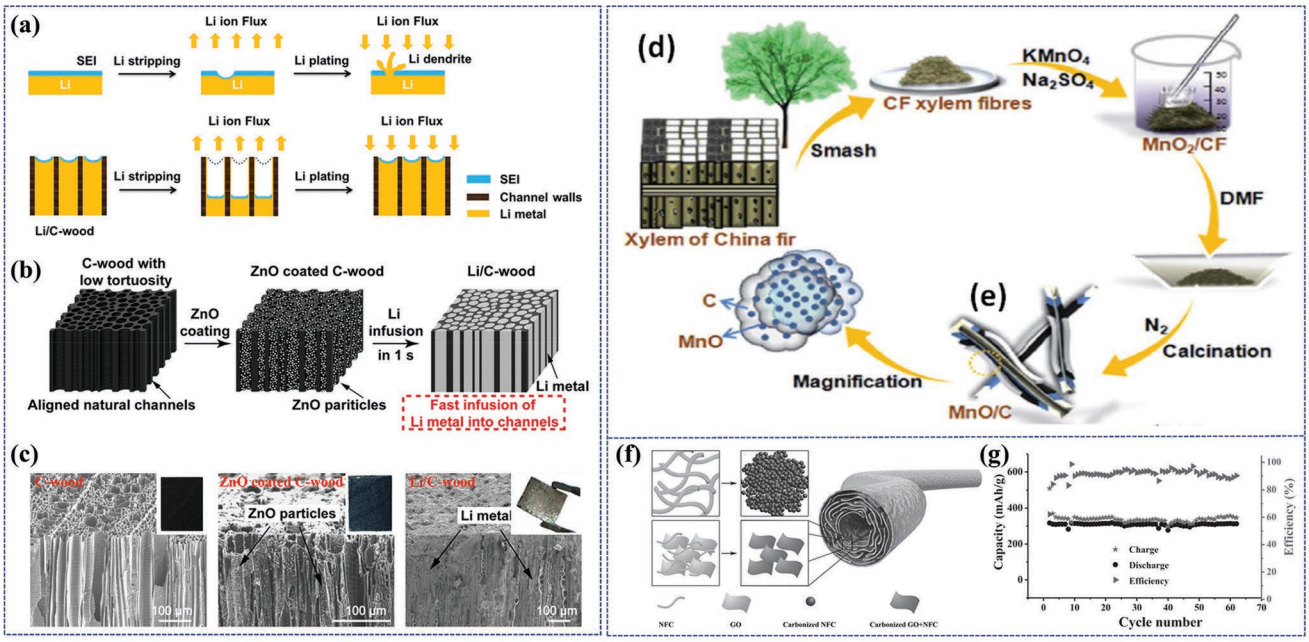


**Figure 8.** a) Schematic illustration of Li stripping/plating behavior for bare Li metal electrodes and Li/C–wood electrodes. b) Fabrication process of the Li/C–wood composite; c) SEM images of C-wood, ZnO-coated C–wood, and Li/C–wood electrodes. The inset shows the corresponding digital images. a–c) Reproduced with permission.[51] Copyright 2017, National Academy of Science. d,e) The fabrication of the MnO/C sample. Reproduced with permission.[52] Copyright 2014, Royal Society of Chemistry. f) Schematic to show the morphology of NFC changed from fibers (before carbonization) to sphere particles after carbonization. g) Charge/discharge capacity and corresponding CE cycled at 25 mA $g^{-1}$. The data are from the second cycle to the 63rd cycle. f–g) Reproduced with permission.[53] Copyright 2014, Wiley-VCH.

capacity of 700 and 1000 mAh $g^{-1}$ at 22 and 50 °C, respectively, at 0.1 C rate. Additionally, Hu's group used the CW with a 3D highly porous (73% porosity) conductive framework as Li host material.[51] The result indicated that the Li/C–wood electrode can be obtained by infusing molten Li metal into the straight channels of C-wood taking advantage of the merits of natural wood (e.g., low tortuosity and high porosity). To increase the wettability between C-wood and Li, the surface of C-wood was coated with a thin layer of ZnO before infusion of molten Li, resulting in a rapid infusion of molten Li into ZnO-coated C-wood channels (**Figure 8**a–c). Therefore, in symmetric cells, the Li/C–wood electrode exhibited more-stable stripping/plating profiles, better cyclic stability (≈150 h at 3 mA $cm^{-2}$) and a lower overpotential (90 mV at 3 mA $cm^{-2}$) compared with bare Li metal electrode.

In addition, Gao's group created a nanocomposite material (MnO/C) with a super low content (5.3 wt%) of MnO on the surface of nanoporous carbon derived from carbonized wood fibers (Figure 8d,e).[52] Owing to the strong synergistic effect between the MnO pseudocapacitance action and the carbon capacitance, the MnO/C anode demonstrated a superior $Li^+$ storage performance with a high discharge capacity of 952 mAh $g^{-1}$ at 0.1 A $g^{-1}$ after 100 cycles, indicating an outstanding cycle stability. Interestingly, Li et al. presented a well-aligned graphene oxide (GO)–NFC hybrid fiber (GO + NFC) with a high conductivity of 649 ± 60 S $cm^{-1}$ by a wet-spinning method and subsequent carbonization.[53] GO used as a template for NFC carbonization to change the morphology of the carbonized NFC, while decreasing the carbonization temperature of NFC (Figure 8f). The as-prepared GO + NFC hybrid fiber was used as a LIBs anode with a stable discharge capacity of 312 mAh $g^{-1}$ (Figure 8g).

### 4.2. Wood as Current Collectors

To achieve high energy density for LIBs, an effective way is to fabricate thick electrodes by reducing the content of nonelectroactive components. However, the main challenges are the poor ionic transport capability and potential electrode deformation in the thick electrode, leading to the electrode cracking and detachment from the current collector.[51] Inspired by the straightly channels of natural wood, a multichannel wood carbon was designed as a 3D current collector with highly conductive, porous, lightweight and low-tortuosity carbon framework (CF) by directly carbonization of natural wood (**Figure 9**a,b).[47] Benefiting from the unique multichannel structure of CF, the ultrahigh $LiFePO_4$ (LFP) mass loading of 60 mg $cm^{-2}$ in CF with a large thickness of 800 μm was achieved. As a result, LFP–CF 3D electrode exhibited an impressive capacity of 7.6 mAh $cm^{-2}$ (95 Ah $L^{-1}$ based on volume), and enhanced mechanical properties, leading to lower deformability. Meanwhile, the LFP–CF 3D electrode showed improved cycling stability and capacity retention (Figure 9c,d). The superior performance of the LFP–CF is ascribed to the unique 3D electrode architecture with a highly conductive, interconnected carbon networks enabling to increase transport of the electrons and ions. More importantly, both the electronic and ionic kinetics are significantly

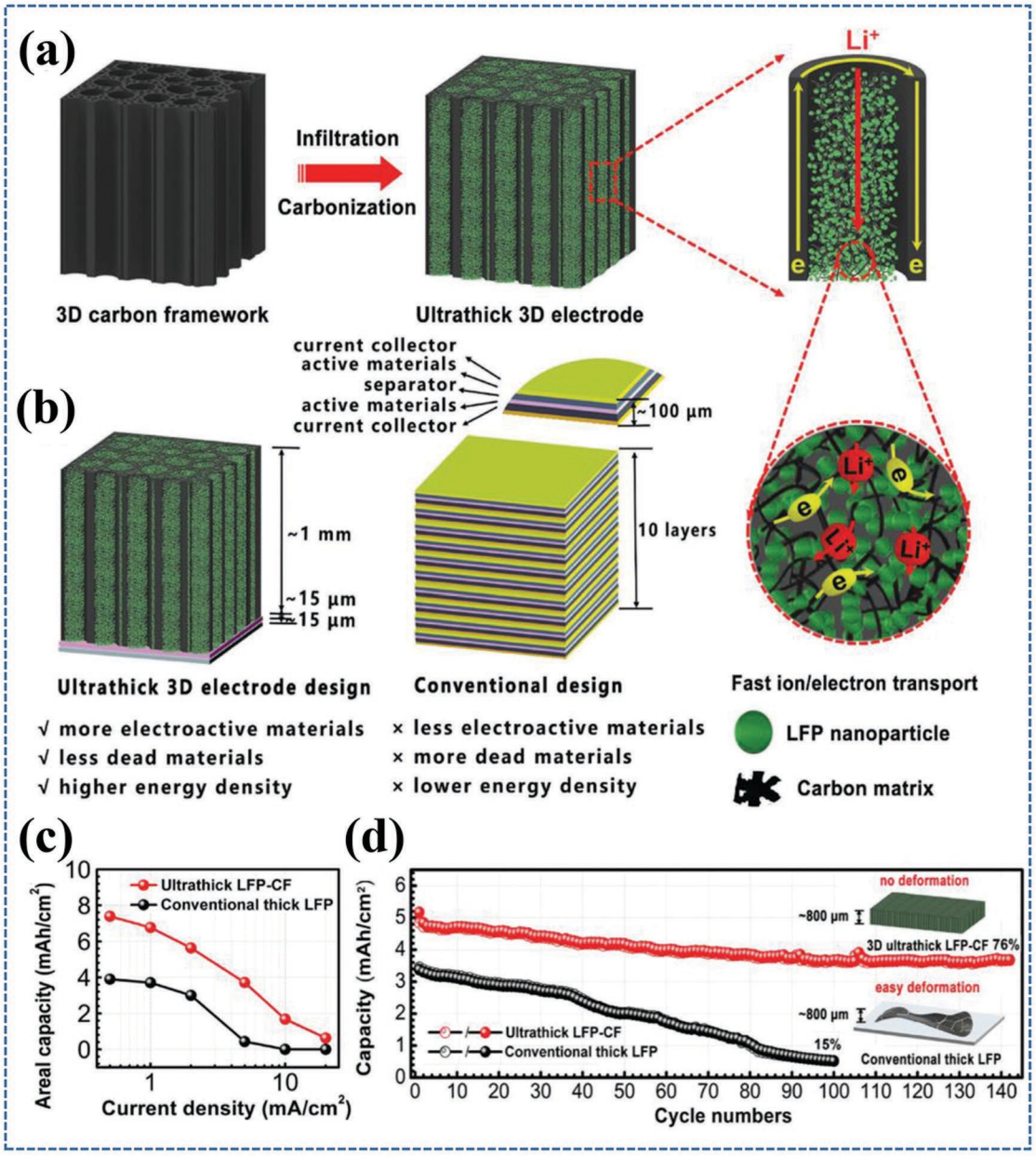


**Figure 9.** a) Schematic illustration of the fabrication for ultrathick 3D electrode. b) Visual comparison between batteries with ultrathick 3D electrode and conventional designs. c) Areal capacity–current density plots and d) cycling performance of the ultrathick LFP–CF electrode and the conventional thick LFP electrode. Insets in (d) illustrate the easy deformation of the conventional thick LFP electrode and the nondeformation of the 3D ultrathick LFP–CF electrode. Reproduced with permission.[47] Copyright 2018, Wiley-VCH.

enhanced, due to the highway of straight channels, resulting in a high-performance for LIBs. Therefore, the work provided a facile yet efficient method to construct ultrathick electrodes by infiltrating the active electrode materials into the straight channels of the 3D current collector. Inspired by this work, we designed CW as a current collector/substrate to grow active electrode materials (e.g., $Co(OH)_2$, $Ni(OH)_2$) using a typical electrodeposition process.[35] Besides, other electrode materials (e.g., $TiO_2$@CW, $SnO_2$@CW, and $WO_2$@CW) with a high theoretical capacity have also been developed by directly using the CW as a current collector. Further efforts to expand and explore these electrode materials applications in electrochemical energy storage including next-generation LIBs are currently in progress in our laboratory.

### 4.3. Wood as Templates

Template method is one of effective methods to synthesize cathode materials for LIBs.[54] Carbonized wood is an ideal template because of the 3D frameworks and unique porous structure. Liu et al. utilized pine wood as a biotemplate to prepare

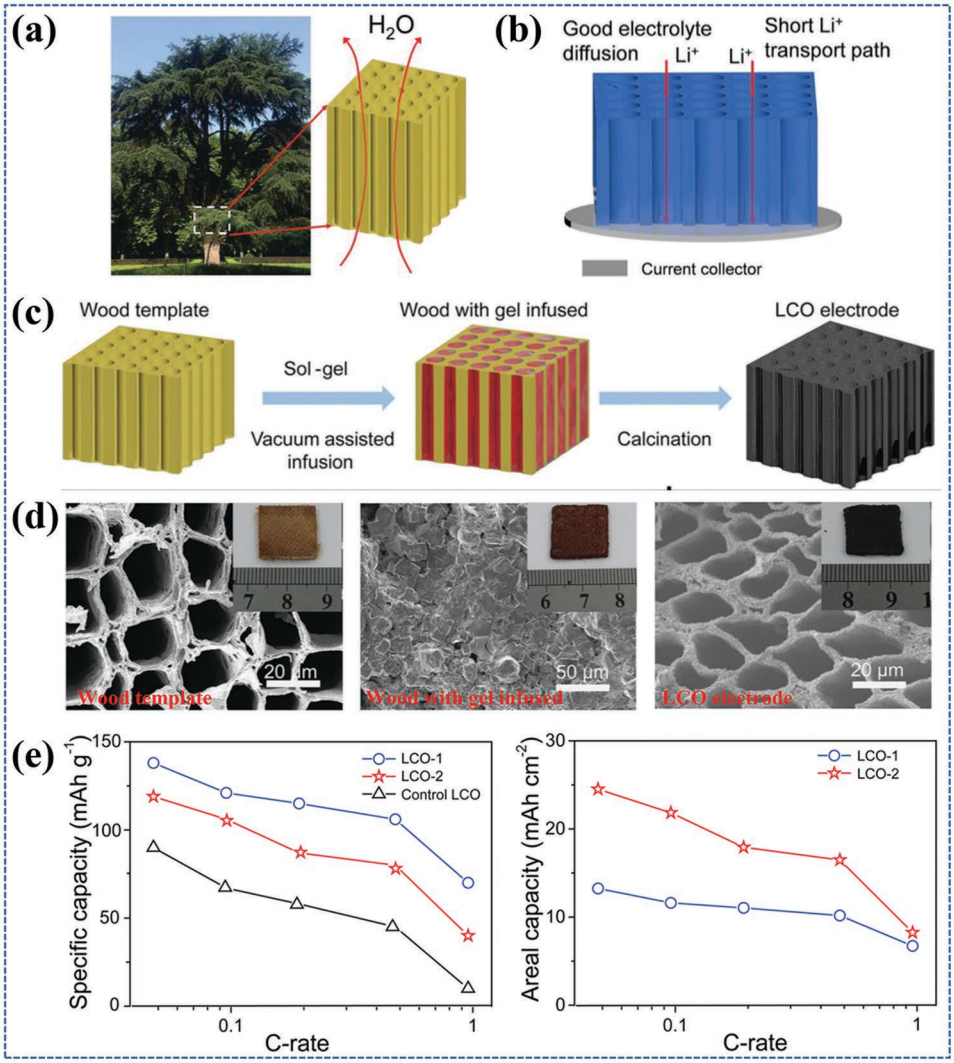


**Figure 10.** a) A photograph of pinewood and illustration of the anisotropic structure. b) Illustration of wood-inspired electrode with vertical channels. c) The illustration of fabrication for ultrathick LCO cathode by wood templating. d) The top view of original wood and LCO-1 material after sol infusion and gel formation. e) Electrochemical performance of LCO cathodes. Reproduced with permission.[57] Copyright 2018, Wiley-VCH.

porous $LiNi_{0.5}Mn_{1.5}O_4$ (LNMO) spinel.[55] This templated LNMO showed a significant enhancement on rate performance compared with the nontemplated LNMO, which was ascribed to the porous structure and highly dispersed active particles. However, commercial LIBs are currently limited the thickness (50–100 μm) of active electrode components (e.g., cathode and anode).[56] Therefore, significant efforts have been afforded to improve the performance of LIBs toward thicker and higher mass loading of electroactive materials. Recently, inspired by the structure of natural wood with the vertical microchannels for the transport of water (**Figure 10**a), Lu et al. used wood as a self-sacrificial template to create ultrathick $LiCoO_2$ (LCO) cathode through a facile sol–gel infiltration and followed by calcination process.[57] The thickness of the as-prepared LCO could be up to 1 mm, and showed a low tortuosity, benefiting to short $Li^+$ transport path and promoting the effective diffusion of electrolyte, thus enhancing the areal capacity and rate performance of LCO cathode (Figure 10b–d). The produced wood-templated LCO cathode exhibited a superior areal capacity of 22.7 mAh $cm^{-2}$ and outstanding rate performance, which are much higher than that commercial LCO cathode (Figure 10e). This work demonstrates a great potential for the low-cost preparation of ultrathick LIBs electrodes via a wood templating sol–gel method.

Despite the use of carbonized woods as anodes, current collectors, and templates have been demonstrated with great potential for high-performance LIBs, there are still some challenges for their practical application, including efficient utilization of hierarchically porous structure of natural wood to improve Coulombic efficiency and cycling stability of LIBs. Besides, the change of surface and interface contact relating to the micro/nanostructure and the composition of wood has a significant effect on the electrochemical performance. Therefore, it is highly desirable to fully investigate the relationship between the hierarchically porous structure and electrochemical performance of wood-based materials, including the transport

of electrons and ions, and reaction kinetics. Moreover, the use of wood-based materials as templates and current collectors for LIBs should be studied in detail from the viewpoint of surface and interface chemistry. Thus, rational design and controllable fabrication of micro/nanostructure for optimization of surface and interface remain a challenge.

## 5. Wood-Derived Materials in Next-Generation Batteries

### 5.1. Lithium–Sulfur Batteries

Lithium–sulfur (Li–S) batteries offer a high theoretical energy density (2600 Wh $kg^{-1}$), which is 3–5 times that of conventional LIBs.[58] Additionally, sulfur is naturally abundant, and low cost, making Li–S batteries particularly attractive compared with LIBs. However, the practical application of Li–S batteries is still limited by a few issues, including the insulating nature of sulfur, volume changes in sulfur (≈80%) during cycling, and the "shuttle effect" caused by the dissolution of intermediate polysulfides ($Li_2S_x$, $4 \le x \le 8$) in organic electrolytes. To address these issues, great efforts have been devoted to design and develop novel electrodes, separators, and electrolytes.[59] Recently, some of wood-based nanomaterials have been developed to construct high performance of Li–S, Li–$O_2$, and Li–$CO_2$ batteries (**Table 3**).

For example, Kaskel and co-workers utilized wood as a template to fabricated a hierarchical carbon monolith by steam or $CO_2$ activation for Li–S batteries.[60] The as-made materials have large specific surface area and hierarchical pores, increasing efficiently ionic transport and Li-storage ability. Recently, Borchardt et al. used a nonpurified wood as a carbon source, $K_2CO_3$ as an activation agent, and urea and/or melamine as a nitrogen source, respectively, to synthesize N-doped carbon by high-energy ball milling and carbonization for Li–S batteries (**Figure 11**a).[61] The obtained N-doped porous carbon showed an extremely high specific surface area (≈3000 $m^2$ $g^{-1}$) and a large pore volume (≈2 $cm^3$ $g^{-1}$), as well as high initial discharge capacity of 1302 mAh $g_{sulfur}^{-1}$ and a capacity retention of >75% within the first 50 cycles (Figure 11b). A 3D ordered porous carbon was also successfully constructed by carbonized wood filled with RGO as an ideal support for high mass loading sulfur (Figure 11c,d).[62] The obtained S@C–wood electrode with a high sulfur loading of 21.3 mg $cm^{-2}$ exhibited a high areal capacity of 15.2 mAh $cm^{-2}$ (Figure 11e). Additionally, natural wood microfiber possesses unique hierarchical and mesoporous structure, which is a promising precursor for porous carbon.[63] The carbonized mesoporous wood fiber (CMWF) was also reported as a host material to support sulfur forming a freestanding electrode. Meanwhile a thin $Al_2O_3$ layer (5 nm) was coated on CMWF to form a functionalized CMWF (f-CMWF), (Figure 11f). The freestanding S/f-CMWF cathode with a high sulfur loading (70 wt%) exhibited an initial capacity of 1115 mAh $g^{-1}$ at 400 mA $g^{-1}$, and still retained a capacity of 859 mAh $g^{-1}$ after 450 cycles (Figure 11g). In addition, cellulose nanocrystals (CNCs) prepared by acid hydrolysis of wood cellulose fibers was also developed as a carbon source to synthesize nanoporous N,S dual-doped carbon materials with a high surface area (Figure 11h).[64] A synergistic effect from N and S heteroatoms on porous carbon as a sulfur host material greatly improved the chemisorption of lithium polysulfides and electric conductivity compared with pure carbon, resulting in a superior cycling stability with a capacity decay rate of 0.052% per cycle (Figure 11i).

**Table 3.** Summary of some parameters of various wood-based materials for next-generation batteries.

| Wood species | Carbonization condition [°C] | Function | Electrochemical performance | Ref. |
|---|---|---|---|---|
| Birch wood | 800/Ar, $CO_2$ | As cathode for Li–S batteries | 580 mAh $g_{sulfur}^{-1}$ at 20 mA $cm^{-2}$ (2 C) | [60] |
| Lignin | 800/$N_2$ | As cathode for Li–S batteries | 1302 mAh $g_{sulfur}^{-1}$, retention of >75%, 50 cycles | [61] |
| Basswood | 1000/Ar; 800/$CO_2$ | Wood carbon/RGO as cathode for Li–S batteries | 15.2 mAh $cm^{-2}$ | [62] |
| Wood fiber | 1000/Ar | As cathode for Li–S batteries | 1115 mAh $g^{-1}$ at 400 mA $g^{-1}$, 859 mAh $g^{-1}$ after 450 cycles | [63] |
| Cellulose nanocrystals | 900/Ar | As cathode for Li–S batteries | 1370 mAh $g^{-1}$ at C/20 | [64] |
| Pine | 240/Air; 800/$NH_3$ | As cathode for Li–$O_2$ batteries | Energy efficiency of 65%, 20 cycles at a discharge depth of 70% | [67] |
| Wood | 1000/Ar | As cathode for Li–$O_2$ batteries | 8.58 mAh $cm^{-2}$ at 0.1 mA $cm^{-2}$ | [68] |
| Poplar wood | 1000/Ar | As cathode for Li–$O_2$ batteries | Energy efficiency of 91.9%, overpassed 87.1% after 100 cycles | [69] |
| Balsa wood | – | As cathode for Li–$CO_2$ batteries | 11 mAh $cm^{-2}$, 200 cycles | [71] |

### 5.2. Lithium–Oxygen Batteries

Compared to LIBs, Li–$O_2$ batteries, which could deliver much higher energy density, have attracted increasing attention as next-generation energy storage systems.[65] However, further improving performance of Li–$O_2$ batteries is very important for their wide applications. The cathode structure plays a decisive role in the performance of Li–$O_2$ batteries associated with oxygen diffusion, $Li^+$ and electron transfer rate, and discharge product growth.[66] The carbonaceous materials have been regarded as a promising candidate for cathode of Li–$O_2$ batteries because of their good mechanical and electrical performance. However, various carbon materials (e.g., graphene, carbon nanotube, and carbon nanofibers) remain to limit the large-scale application due to expensive and complicated preparation procedures. Additionally, the electrochemical performances of the whole device are still very low, owing to the existence of nonelectroactive components. Therefore, wood carbon offers an

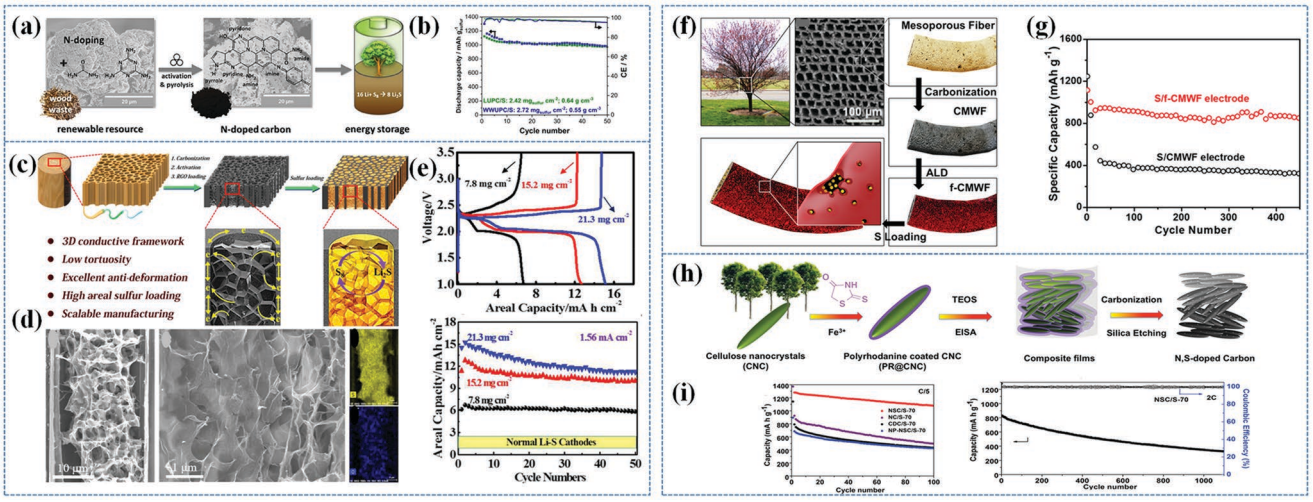


**Figure 11.** a) Schematic diagram of nitrogen-doped porous carbon as an electrode material for lithium–sulfur batteries. b) Comparison of cycling performance at C/10 for LUPC/S and WWUPC/S composites. a,b) Reproduced with permission.[61] Copyright 2019, Wiley-VCH. c) Schematic illustration of the preparation process and structure of the S@C–wood composite electrode. d) SEM images and elemental mappings for the S@C–wood composite. e) Electrochemical performance of the S@C–wood electrode: GCD curves and cycling performance of the S@C–wood electrode with different sulfur mass loadings. c–e) Reproduced with permission.[62] Copyright 2017, Wiley-VCH. f) Schematic of the hierarchical and mesoporous structure of natural wood fiber. g) Cycling stability test of S/CMWF electrodes and S/f-CMWF electrodes. f,g) Reproduced with permission.[63] Copyright 2017, American Chemical Society. h) The schematic illustration of synthesis on nitrogen/sulfur-doped cellulose (NSC); i) the long-term cycling performance of NSC/S-70 electrode at 2 C rate, showing Coulombic efficiency on the left *y*-axis. h,i) Reproduced with permission.[64] Copyright 2015, Wiley-VCH.

attractive potential for large-scale fabrication of self-standing porous carbon electrodes in Li–$O_2$ batteries.

Luo et al. synthesized a wood-derived porous carbon (wd-C) by two-step carbonization, using as freestanding cathode for Li–$O_2$ batteries.[67] The wd-C showed hierarchically porous structure of natural wood, facilitating both mass transport and discharge product storage. In addition, the wood-derived N-doped carbon (wd-NC) was also prepared at 800 °C for 2 h under anhydrous $NH_3$. The wd-NC electrode significantly increased the overall energy density of device due to the absence of additional current collectors and binders. Moreover, the N-doping further enhanced the catalytic activity of the carbon cathode with lower overpotential and higher capacity in Li–$O_2$ batteries. To further improve performance, various catalysts have been introduced into carbon cathode in Li–$O_2$ batteries. a "breathable" wood-based cathode was designed for Li–$O_2$ batteries.[68] The carbonized and activated wood (CA-wood) acted as a host for depositing ruthenium nanoparticles (Ru NPs) catalyst (CA-wood/Ru) as a cathode in Li–$O_2$ batteries (**Figure 12**a). The Ru NPs were well dispersed on the porous wall of the ordered microchannels, which was beneficial to provide numerous reactive sites. Moreover, the highly porous walls on the microchannels can also enable the impregnation by electrolyte, forming continuous thin electrolyte layers for fast $Li^+$ transport. As a result, a high specific area capacity of 8.58 mAh $cm^{-2}$ at 0.1 mA $cm^{-2}$ and superior cycle performance for CA-wood/Ru cathode (thickness: ≈700 µm) could be achieved (Figure 12b). Similarly, Zhu et al. reported that a wood-derived cathode was obtained from natural wood by carbonization, activation, and then loading of $RuO_2$ nanoparticles as catalysts ($RuO_2$/WD-C) for Li–$O_2$ batteries (Figure 12d).[69] As shown in Figure 12e,f, the specific areal capacity of the assembled batteries using $RuO_2$/WD-C cathode was better than 8 mAh $cm^{-2}$ and the charge terminal potential was lower than 3.8 V at 0.1 mA $cm^{-2}$. The energy efficiency was enhanced up to 91.9% and overpassed 87.1% after 100 cycles. Furthermore, the $RuO_2$/WD-C cathode could be completely regenerated after a deep charge–discharge cycle by simply washing with water.

Most recently, Chen et al. reported a tri-pathway design concept by nature inspired for flexible Li–$O_2$ batteries.[70] Natural wood (balsa) was used directly to fabricate a continuous tri-pathway structure by facile chemical delignification and a CNT/Ru coating process for the noncompetitive transport of electrons, $Li^+$ ions, and $O_2$ gas (**Figure 13**a,b). This approach avoids high-temperature thermal treatment to make wood electrically conductive while without sacrificing the mechanical robustness or flexibility of wood. Continuous electron transport through the surface-coated CNT network, ion transport along the nanoporous in cell walls, and $O_2$ gas transport through the intrinsic wood channels constitute the noncompetitive triple pathways through the flexible wood cathode (Figure 13e). The Ru nanoparticles loading on the surface of the CNTs improves the redox reactions within the cathode (Figure 13d). The noncompetitive triple pathway design concept endowed the CNT/Ru-coated F-Wood cathode with a low overpotential of 0.85 V at 100 mA $g^{-1}$, a high areal capacity of 67.2 mAh $cm^{-2}$, a long cycling life of 220 cycles, and superior mechanical stability. The integration of such excellent electrochemical performance, outstanding mechanical flexibility, and renewable yet cost-effective starting materials via a nature-inspired design opens new opportunities for developing portable energy storage devices.

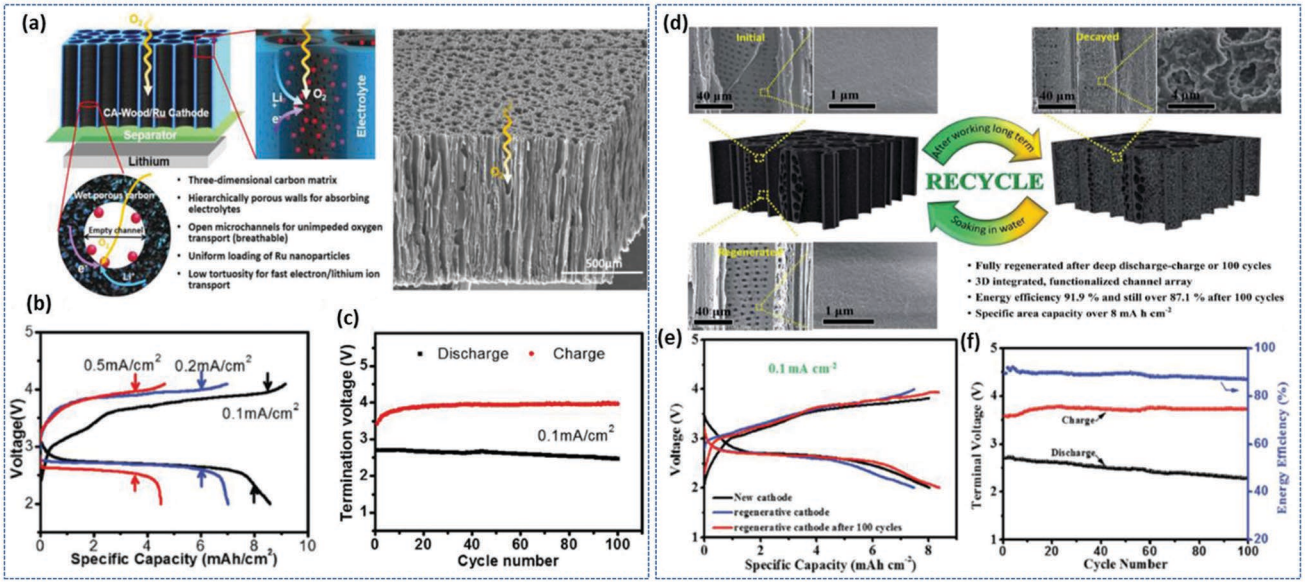


**Figure 12.** a) Schematic diagram of the Li–$O_2$ batteries with the CA-wood/Ru cathode with hierarchically porous, open, and low-tortuosity microchannels. Electrochemical performance of the Li–$O_2$ battery with the CA-wood/Ru cathode: b) charge/discharge curves; c) termination voltages of charge and discharge with cycle numbers. a–c) Reproduced with permission.[68] Copyright 2017, Wiley-VCH. d) Schematic diagram of the $RuO_2$/WD-C cathode structure and the regenerative process. e) The charge–discharge curves of the $RuO_2$/WD-C cathode at 0.1 mA $cm^{-2}$. f) Termination voltages of charge, discharge, and specific energy efficiency with cycle numbers. d–f) Reproduced with permission.[69] Copyright 2018, Royal Society of Chemistry.

### 5.3. Lithium–$CO_2$ Batteries

The Li–$CO_2$ battery has aroused increasing attentions, since it was firstly reported by Archer et al.[71] The work mechanism of Li–$CO_2$ battery is similar to a natural tree, which breathes in $CO_2$ to produce organic compounds via photosynthesis (**Figure 14**a). The Li–$CO_2$ battery uses $CO_2$ gas as a cathode fuel for energy storage according to the reaction of $3CO_2 + 4Li^+ + 4e^- \rightarrow 2Li_2CO_3 + C$. The Li–$CO_2$ battery is considered a promising candidate to capture $CO_2$ because of its ability to convert the captured $CO_2$ to energy and storage. In the past few years, despite significant progress has been made for construction of Li–$CO_2$ battery, the Li–$CO_2$ battery is still face several challenges including the stable discharge product, the slow kinetics of $CO_2$ reduction, and the slow diffusion of electrolyte and $CO_2$ gas.

Recently, a flexible wood-based cathode was developed for Li–$CO_2$ battery with high reversible capacity, good flexible, and highly rechargeable (Figure 14b).[72] The flexible wood-based cathode was prepared via a facile chemical treatment process, followed by coating with a Ru/CNT composites. Notably, the modified wood-based cathode exhibited excellent flexibility compared with pristine wood (Figure 14c,d). A Li–$CO_2$ battery was fabricated by using the flexible wood modified with Ru/CNT catalysts as a cathode and Li foil as an anode. Benefiting from the unique channel structure of nature wood, both $CO_2$ gas and electrolyte can fast transport and effectively reaction with the Ru/CNT catalysts, resulting in a significantly enhanced electrochemical performance. The assembled Li–$CO_2$ battery showed a low overpotential of 1.5 V and a high discharge capacity of 11 mAh $cm^{-2}$, and long cycling stability (Figure 14e). Such a wood-based Li–$CO_2$ battery displays a promising candidate for $CO_2$ capture/utilization and wearable energy storage devices.

### 5.4. Sodium-Ion Batteries

NIBs have recently received great attentions due to its low-cost, and easily availability compared with LIBs.[73] Many anode materials for NIBs have been developed, such as hard carbon, alloys and metal oxides. Among them, hard carbon is considered as the most promising candidate because of its lower work potential and relatively higher specific capacity. However, the commercial application of hard carbon anode is impeded by low cycle life and poor rate performance. Therefore, the development of suitable anode materials is critical for improving the performance of NIBs. The representative wood-derived materials to fabricating NIBs are summarized in **Table 4**.

CNFs-derived from wood-cellulose nanofibers have many advantages, including excellent electrical conductivity, thermal and chemical stability, and high Na-storage performance as anode materials for NIBs. For example, Luo et al. prepared a CNFs material directly from cellulose nanofibers though a pyrolysis strategy.[74] Benefiting from high specific surface and 1D nanostructure of the CNFs, the CNFs used as an NIBs anode exhibited a high reversible capacity (255 mAh $g^{-1}$ at 40 mA $g^{-1}$), a superior rate performance (85 mAh $g^{-1}$ at 2 A $g^{-1}$, and an excellent cycling stability (180 mAh $g^{-1}$ at 200 mA $g^{-1}$ over 600 cycles). Additionally, a binder-free anode composed of a layer Sn thin film coated on a conductive wood fiber substrate/current collector was prepared

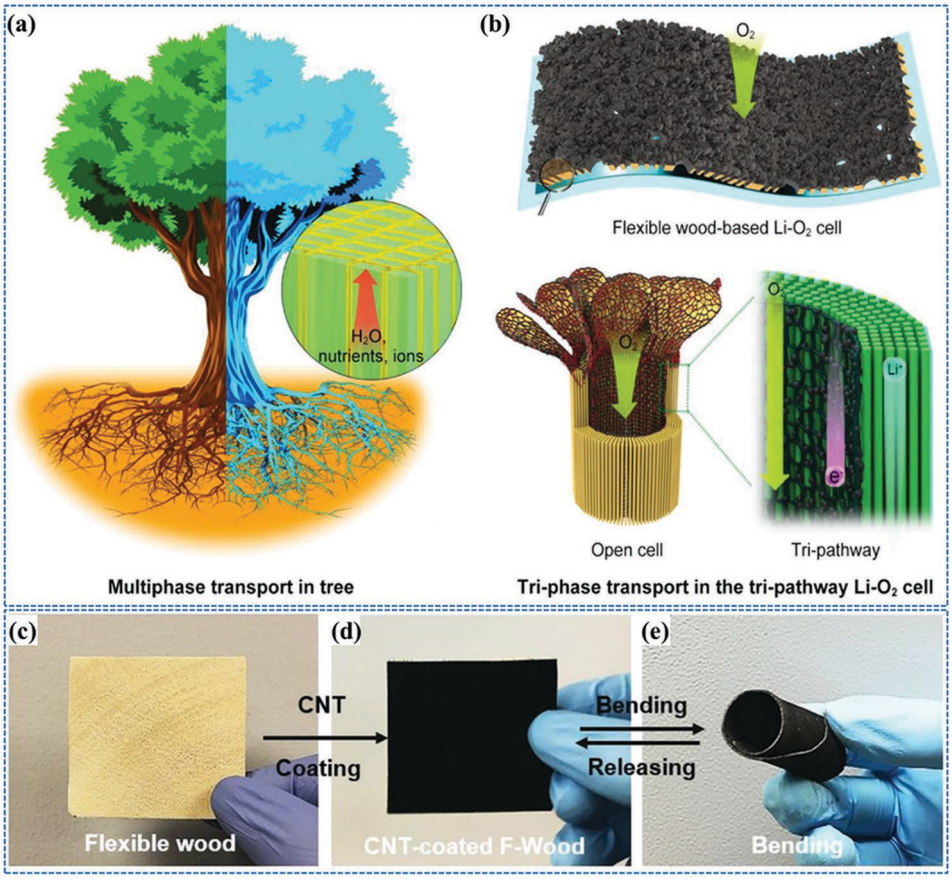


**Figure 13.** Schematic illustration of the tree-inspired tri-pathway design for flexible Li–$O_2$ cells. a) Multiphase transport (e.g., water, ions, and nutrients) is essential for photosynthesis in trees. b) A tri-pathway structural design was realized by chemically treatment and subsequent CNT/Ru coating process to enable the noncompetitive triphase transport of $Li^+$ ions, electrons, and oxygen gas. c–e) Photographs of the c) original flexible wood, d) CNT-coated flexible wood, and e) bent CNT-coated flexible wood membranes. Reproduced with permission.[70] Copyright 2019, Wiley-VCH.

by an electrodeposition method.[75] The active Sn thin film showed good electrical contact with the current collector, while the wood fibers provided a lightweight substrate with high mechanical performance, large special surface area, and a porous structure, enabling effectively transport of ions and electrons. As a result, the Sn@WF anode of NIBs delivered an initial specific capacity of 339 mAh $g^{-1}$ and after 400 cycles without performance decay. In addition, Zhu and co-workers reported another carbon anode of NIBs by the carbonization of ordered CNCs (**Figure 15**a–c).[76] The CNCs derived porous carbon presented superior performances with a high reversible capacity of 340 mAh $g^{-1}$ at 100 mA $g^{-1}$, and good cycling stability holding 88.2% capacity over 400 cycles (Figure 15d), which is attributed to the high electrical conductivity, porous structure, and larger interlayer spacing. Moreover, the same research group designed a NIBs carbon anode with a 3D porous structure by directly carbonizing natural wood.[77] The carbonized wood showed numerous mesopores in the horizontal direction and many straight channels in the vertical direction (Figure 15e). Benefiting from the unique structure of natural wood, an ultrathick wood carbon anode (850 µm) with a large active mass loading (55 mg $cm^{-2}$) delivered a high areal capacity of 13.6 mAh $cm^{-2}$ (Figure 15f). When assembling a full cell we used the wood carbon as a freestanding anode and a suited $Na_3V_2(PO_4)_3$ as a cathode. The full cell exhibited an outstanding cycling performance with a capacity retention rate of >95% over 350 cycles (Figure 15g). However, further optimization of the cathode material is necessary to better suit the ultrathick wood-based carbon anode for achieving a high energy density for NIBs in the future.

Very recently, Zheng et al. reported a NIB based on a couple with the $Na[Cu_{1/9}Ni_{2/9}Fe_{1/3}Mn_{1/3}]O_2$ (NCNFM) as cathode material and a hard carbon as anode material.[78] This hard carbon was made by a one pot high temperature pyrolysis of poplar wood (PHC1400). The full NIBs delivered an outstanding reversible specific energy of 212.9 Wh $kg^{-1}$ at 1 C, and 165.8 Wh $kg^{-1}$ at 5 C, respectively and a long cycle life of 1200 cycles. The superior performance might be attributed to the high specific capacity of ≈330 mAh/g and the ICE of 88.3% for the hard carbon. Moreover, when used as a cathode mass loading of 20.5 mg $cm^{-2}$ (≈2 mAh $cm^{-2}$), which met the demand of industrial application, the coin cell showed excellent specific energy and long cycling stability with a capacity retention rate of about 94% after 600 cycles at 2 C (Figure 15h). More importantly, the capacity and the voltage plateaus could be completely recovered after 1400 cycles when setting the current rate

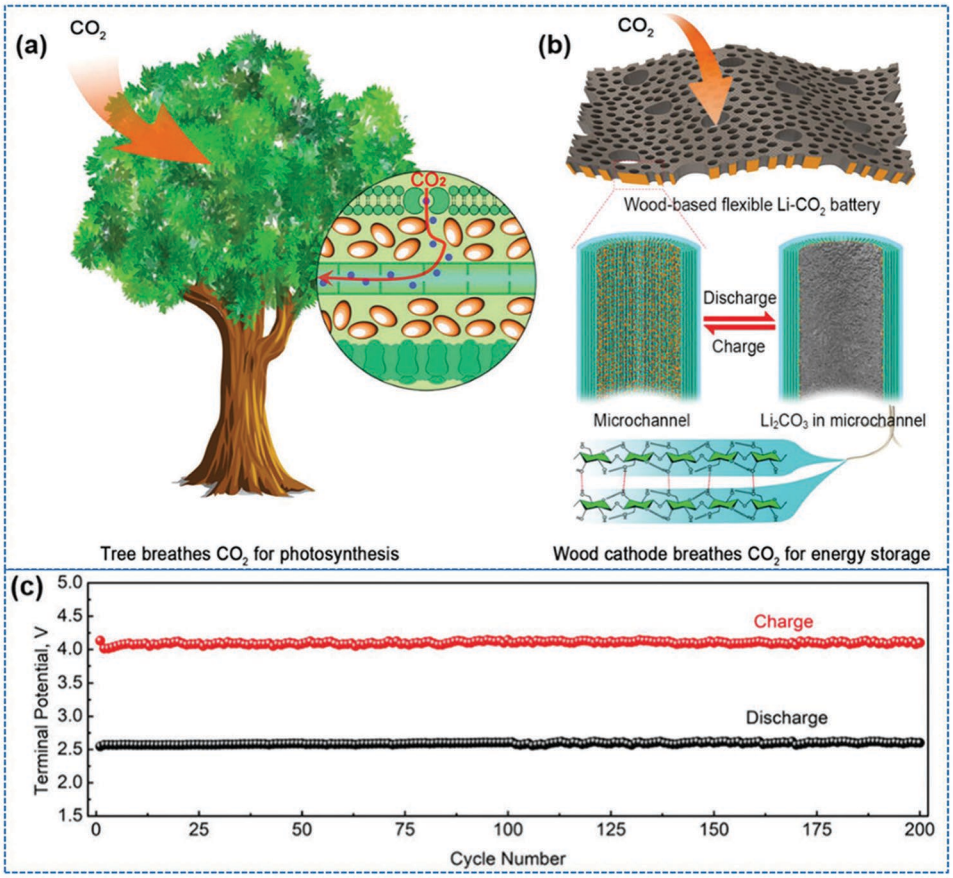


**Figure 14.** Schematics showing the nature-inspired Li–$CO_2$ battery design. a) The schematic of a plant absorbing $CO_2$ for photosynthesis; b) the schematic of the Li–$CO_2$ battery based on the flexible wood cathode; morphology and microstructure of the flexible wood-based cathode; c) photos of the pristine balsa wood and d) the flexible cathode after introducing the CNT-coated Ru catalyst; e) terminal voltage of each charge (red) and discharge (black) showing almost no change over 200 cycles. Reproduced with permission.[72] Copyright 2018, Royal Society of Chemistry.

of C/10 (Figure 15i), which was very important for practical applications. This work suggests that the cathode and anode materials are becoming mature and this is an emerging start for industrial application of NIBs.

Encouraging advance has been made regarding the use of wood-derived materials in next-generation batteries (e.g., Li–S, Li–$O_2$, Li–$CO_2$, and NIBs); however, there are still several significant issues to be resolved for practical applications. For example, the sulfur mass loading still needs to be increased in the 3D wood-derived electrodes of Li–S batteries to obtain high energy density, while retaining superior electrical conductivity and long operational life. In Li–$O_2$ batteries, to date, few studies focus on engineering wood-based electrode structures to fabricate multipathways for the highly effective transport of $Li^+$ ions, electrons, and $O_2$ gas. Additionally, the cycle stability and energy efficiency should be further increased. Achieving

**Table 4.** Summary of some parameters of various wood-based materials for NIBs.

| Wood species | Carbonization condition [°C] | Function | Electrochemical performance | Ref. |
|---|---|---|---|---|
| Softwood kraft pulp-derived CNF | 1000/Ar | CNF-derived carbon as anode | 255 mAh $g^{-1}$ at 40 mA $g^{-1}$, 85 mAh $g^{-1}$ at 2000 mA $g^{-1}$, 176 mAh $g^{-1}$ at 200 mA $g^{-1}$ over 600 cycles | [74] |
| Wood fibers | 100/$N_2$ | Wood fibers as support/substrate | 339 mAh $g^{-1}$, 400 cycles | [75] |
| CNCs | 1000/Ar | Derived porous carbon as anode | 340 mAh $g^{-1}$ at 100 mA $g^{-1}$, 88.2% capacity for 400 cycles | [76] |
| Hard wood block | 1000/Ar | Wood carbon as anode | 13.6 mAh $cm^{-2}$ | [77] |
| Poplar wood | 1400/Ar | Derived hard carbon as anode | 212.9 Wh $kg^{-1}$ at 1 C, 165.8 Wh $kg^{-1}$ at 5 C, 1200 cycles, ≈330 mAh $g^{-1}$, ICE = 88.3% | [78] |

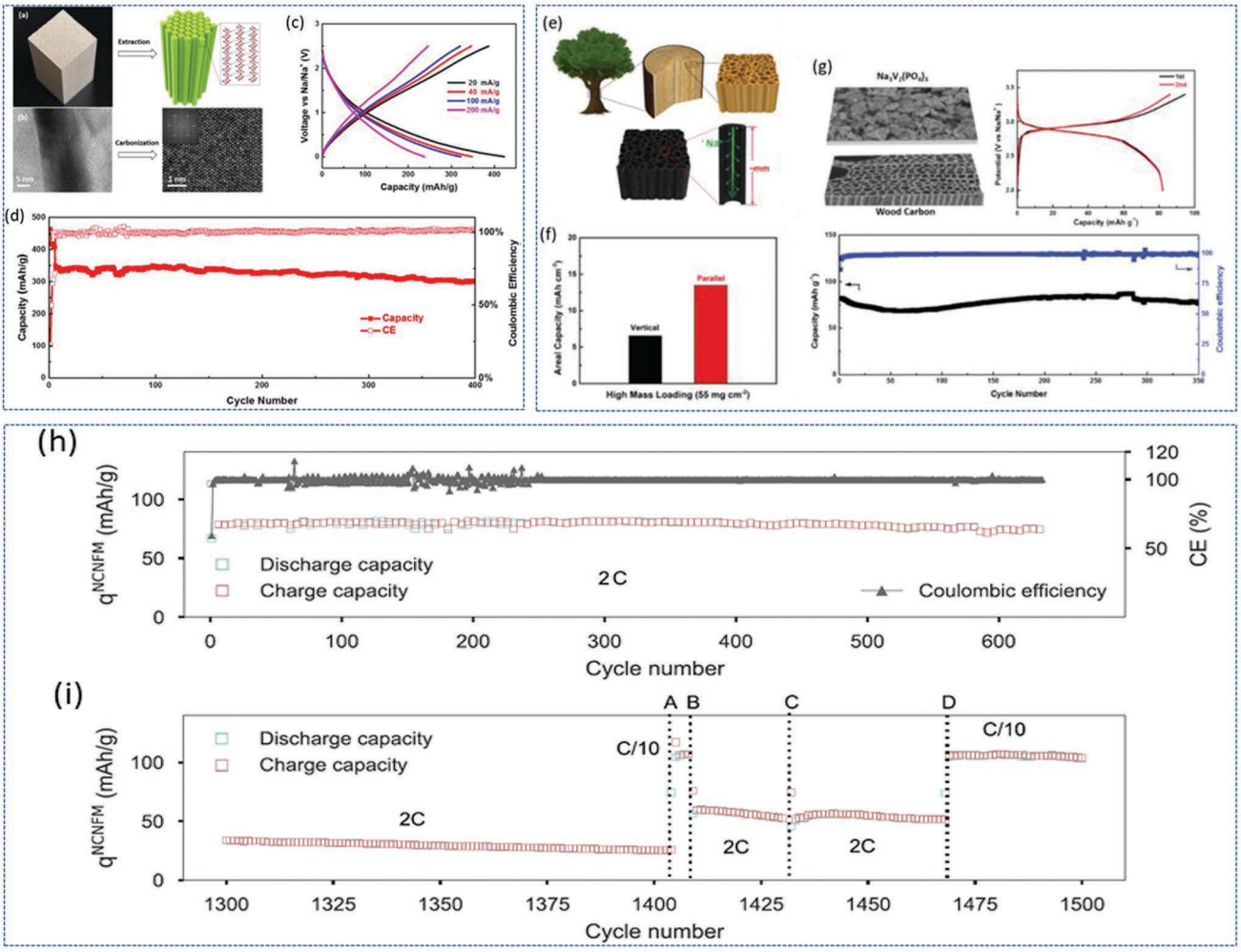


**Figure 15.** a) Photograph of a wood block (left) and the schematic of CNC molecular structure extracted from wood (right); b) high-resolution transmission electron microscopy (HRTEM) images of CNC before (left) and after carbonization (right), respectively; electrochemical performances of carbonized CNC: c) galvanostatic charge/discharge profiles (GCD); d) cycling performance at 10 mA $g^{-1}$ for the first five cycles and then 100 mA $g^{-1}$, corresponding CE in the right *y*-axis. a–d) Reproduced with permission.[76] Copyright 2017, Elsevier. e) Schematic to show a piece of unique anisotropic natural wood with well-defined channels along the tree growth direction; f) Na-ion storage comparison of vertical cutting and parallel cutting wood carbons with a large thickness. g) Schematic showing a full cell with low tortuosity wood carbon anode and $Na_3V_2(PO_4)_3$ cathode; charge/discharge curves, and long-term cycling performance. e–g) Reproduced with permission.[77] Copyright 2016, Wiley-VCH. The industrial level mass loading full-cell performance: h) cycling performance of 2 C rate and i) primarily decay analyzing at 2 C rate. The mass loading was about 7 mg $cm^{-2}$ (ratio of the active material was 95%) and 20.5 mg $cm^{-2}$ (ratio of the active material was 93%), respectively, for the anode and the cathode. h–i) Reproduced with permission.[78] Copyright 2018, Elsevier.

a low overpotential for the wood-based air cathode for Li–$CO_2$ battery still remains challenging. Developing wood-carbon anodes in SIBs with high specific energy, superior rate performance, and long cycle life is still highly desirable.

Therefore, more approaches to rational design of wood-derived porous structures are vital to the development of next-generation high-performance energy storage devices. In particular, the combination of theoretical calculations and experimental measurements is necessary to better understand the correlations between wood-derived porous structures and their electrochemical behavior in energy storage devices, providing scientific basis for knowledge-based design of electrode materials for high-performance devices.

## 6. Conclusion and Prospects

In this review, we have reviewed recent developments in wood and its derivative materials for EES techniques, including SCs, and rechargeable batteries.

Significantly progress has been achieved for wood-based EES electrodes and devices, especially with ultrahigh mass loading for thick electrode design, however, several challenges still remain (**Figure 16**) and need to further overcome including 1) efficient utilization of hierarchically porous structure of natural wood is still a challenge for EES. Very small pores hinder electrolyte ions accessibility, but too large pores decrease the volumetric energy density and capacitance of energy storage


**Figure 16.** A brief summary of challenges and future research directions for new-generation energy storage and conversion devices based on wood-derived materials.

device, because the void space could not be fully used. Thus, the pore sizes of electrode material should be slightly larger than the sizes of solvated electrolyte ions; 2) the surface/interface chemistry of wood-derived materials needs to be studied in detail. The wood framework needs a compact, continuous and strong contact with electroactive components, meanwhile keeping a low resistance of the interface. On the other hand, the electroactive materials should be homogeneously filled into the pores of wood as much as possible to decrease the "dead volume" of electrode materials; 3) it is highly desirable but challenging to make wood-based materials with both attractive electrochemical performance and desirable mechanical properties (e.g., strength, toughness, and flexibility); 4) large-scale application is still limited by the electrochemical performance and production cost of wood-based materials; 5) greener functionalization and treatment of wood are desired for total procedure sustainable development; 6) expanding more wood species utilized is highly desirable but still limited.

Based on the above challenges/critical issues, some possible strategies are suggested as follows: 1) new strategies to engineer pore sizes of wood-derived materials should be developed. Numerous micro/mesopores can be created by activation of wood, benefiting to increase specific surface area. The macropores of wood can be efficiently become small by modifying inner surface of wood walls or filling desirable gust materials into pores. 2) For improving surface/interface chemistry, one strategy is the development of in situ growth of active electrode materials on outer and inner surface of wood walls, such as hydrothermal, electrodeposition, and ALD strategies. Another efficient method is functionalization of wood before decoration of active electrode materials to improve the interface compatibility for wood-based materials, leading to the stronger surface/interface coupling between the wood and active materials, such as surface coating strategy. 3) Removing partial components (e.g., lignin, hemicellulose) of wood, or forming composites with some polymers (e.g., resins), followed by post treatment (e.g., carbonization, hot-pressing) can significantly improve the mechanical performances of wood-based materials. 4) Design of thick and self-standing electrode (without the need for current collectors or any additional conductive additive/adhesives) is an effective method to enhance electrochemical performance of wood-based materials. 5) Environmentally friendly chemicals used to treat/modify wood, milder carbonized wood conditions, and simper fabrication process of electrode material and device should be further developed. 6) Seeking general and universal synthetic approaches of wood-derived materials are highly desirable for different wood species.

Therefore, several new research directions should be considered for the development of next-generation energy storage and conversion devices based on wood-derived materials (Figure 16).

(1) It is highly desirable to systemically investigate the relationship between the hierarchically porous structure and electrochemical performance of wood-based materials. As the optimization of pore sizes engineering often delivers an improvement in performances. Thus, further studies should focus on their relationship, including the transport of electrons and ions, and reaction kinetics.
(2) Modification and functionalization of wood for creating the nanocomposites need to be studied from the viewpoint of surface/interface chemistry, and a rational design and controllable fabrication for micro/nanostructure of the surface/interface by the corresponding composited strategies should be further developed.
(3) More efforts need to make wood-based materials to simultaneously have superior electrical conductivity and high mechanical performances (e.g., strength, toughness and flexibility) of the EES device, representing a promising direction for the development of wearable and portable energy storage devices for a sustainable society.
(4) More attention should be given to improve the performance from the whole device level for practical applications.

Thick electrode design with high mass loading is a promising direction to further improve the energy density of device.

(5) Advanced cutting technology of wood and low-cost, greener production should be further developed for large-scale applications based on wood-derived materials.

(6) Advanced assembling and integration techniques are highly desirable for development of next-generation energy storage and conversion devices based on wood-derived materials.

(7) Development of multiscale modeling and simulation are necessary to obtain rational designs of better electrode materials and device configurations for high performance.

Where challenges and opportunities are of coexistence, some challenges need to be overcome. While the research of wood-based materials is still at its infancy stage, it is strongly believed that wood-derived materials will provide a promising potential for EES materials and devices toward the practical use in the near future.

## Acknowledgements

J.H. and B.Z. contributed equally to this work. This work was supported by the National Natural Science Foundation of China (No. 21403274, 11474101, and 91745203), the Fundamental Research Funds for the Central Universities (2015ZM151, 2018PY11, and D2170390), the Chinese Education Ministry Key Laboratory of Resource Chemistry, and the Guangdong Innovative and Entrepreneurial Research Team Program (No. 2014ZT05N200), and the US National Science Foundation under award number DMR-1742828.

## Conflict of Interest

The authors declare no conflict of interest.

## Keywords

batteries, energy storage devices, supercapacitors, wood, wood-derived materials

Received: March 18, 2019
Revised: May 9, 2019
Published online: June 6, 2019

[1] a) J. W. Choi, D. Aurbach, *Nat. Rev. Mater.* **2016**, *1*, 16013; b) P. Simon, Y. Gogotsi, B. Dunn, *Science* **2014**, *343*, 1210; c) W. Lv, Z. Li, Y. Deng, Q.-H. Yang, F. Kang, *Energy Storage Mater.* **2016**, *2*, 107.

[2] M. Armand, J.M. Tarascon, *Nature* **2008**, *451*, 652.

[3] a) Z. N. Yu, L. Tetard, L. Zhai, J. Thomas. *Energy Environ. Sci.* **2015**, *8*, 702; b) J. Han, W. Wei, C. Zhang, Y. Tao, W. Lv, G. Ling, F. Kang, Q.-H. Yang, *Electrochem. Energy Rev.* **2018**, *1*, 139.

[4] D. Larcher, J.-M. Tarascon, *Nat. Chem.* **2015**, *7*, 19.

[5] F. Jiang, T. Li, Y. Li, Y. Zhang, A. Gong, J. Dai, E. Hitz, W. Luo, L. Hu, *Adv. Mater.* **2018**, *30*, 1703453.

[6] C. Chen, L. Hu, *Acc. Chem. Res.* **2018**, *51*, 3154.

[7] a) C. E. Byrne, D. C. Nagle, *Carbon* **1997**, *35*, 267; b) C. E. Byrne, D. C. Nagle, *Carbon* **1997**, *35*, 259.

[8] a) F.-C. Wu, R.-L. Tseng, C.-C. Hu, C.-C. Wang, *J. Power Sources* **2004**, *138*, 351; b) F.-C. Wu, R.-L. Tseng, C.-C. Hu, C.-C. Wang, *J. Power Sources* **2005**, *144*, 302.

[9] D. Klemm, B. Heublein, H. P. Fink, A. Bohn, *Angew. Chem., Int. Ed.* **2005**, *44*, 3358.

[10] Y. Li, E. Vasileva, I. Sychugov, S. Popov, L. Berglund, *Adv. Opt. Mater.* **2018**, *6*, 1800059.

[11] L. A. Berglund, I. Burgert, *Adv. Mater.* **2018**, *30*, 1704285.

[12] H. Zhu, W. Luo, P. N. Ciesielski, Z. Fang, J. Zhu, G. Henriksson, M. E. Himmel, L. Hu, *Chem. Rev.* **2016**, *116*, 9305.

[13] A. C. O'sullivan, *Cellulose* **1997**, *4*, 173.

[14] a) E. Sjostrom, *Wood Chemistry: Fundamentals and Applications*, Academic Press, San Diego, CA **1993**; b) A. P. Russell, L. G. Richard, *Formation and Structure of Wood*, American Chemical Society, Washington, DC **1984**.

[15] M. Zhu, J. Song, T. Li, A. Gong, Y. Wang, J. Dai, Y. Yao, W. Luo, D. Henderson, L. Hu, *Adv. Mater.* **2016**, *28*, 5181.

[16] C. Jia, C. Chen, Y. Kuang, K. Fu, Y. Wang, Y. Yao, S. Kronthal, E. Hitz, J. Song, F. Xu, B. Liu, L. Hu, *Adv. Mater.* **2018**, *30*, 1801347.

[17] Y. Li, Q. Fu, S. Yu, M. Yan, L. Berglund, *Biomacromolecules* **2016**, *17*, 1358.

[18] Y. Li, S. Yu, J. G. Veinot, J. Linnros, L. Berglund, I. Sychugov, *Adv. Opt. Mater.* **2017**, *5*, 1600834.

[19] E. Vasileva, Y. Li, I. Sychugov, M. Mensi, L. Berglund, S. Popov, *Adv. Opt. Mater.* **2017**, *5*, 1700057.

[20] W. Gan, L. Gao, S. Xiao, W. Zhang, X. Zhan, J. Li, *J. Mater. Sci.* **2017**, *52*, 3321.

[21] Z. Yu, Y. Yao, J. Yao, L. Zhang, Z. Chen, Y. Gao, H. Luo, *J. Mater. Chem. A* **2017**, *5*, 6019.

[22] M. Zhu, Y. Li, F. Chen, X. Zhu, J. Dai, Y. Li, Z. Yang, X. Yan, J. Song, Y. Wang, E. Hitz, W. Luo, M. Lu, B. Yang, L. Hu, *Adv. Energy Mater.* **2018**, *8*, 1701028.

[23] T. Li, H. Liu, X. Zhao, G. Chen, J. Dai, G. Pastel, C. Jia, C. Chen, E. Hitz, D. Siddhartha, R. Yang, L. Hu, *Adv. Funct. Mater.* **2018**, *28*, 1707134.

[24] K. K. Liu, Q. Jiang, S. Tadepalli, R. Raliya, P. Biswas, R. R. Naik, S. Singamaneni, *ACS Appl. Mater. Interfaces* **2017**, *9*, 7675.

[25] H. Liu, C. Chen, H. Wen, R. Guo, N. A. Williams, B. Wang, F. Chen, L. Hu, *J. Mater. Chem. A* **2018**, *6*, 18839.

[26] J. Song, C. Chen, C. Wang, Y. Kuang, Y. Li, F. Jiang, Y. Li, E. Hitz, Y. Zhang, B. Liu, A. Gong, H. Bian, J. Y. Zhu, J. Zhang, J. Li, L. Hu, *ACS Appl. Mater. Interfaces* **2017**, *9*, 23520.

[27] R. O. Ritchie, *Nat. Mater.* **2011**, *10*, 817.

[28] Y. Wang, M. Chen, F. Zhou, E. Ma, *Nature* **2002**, *419*, 912.

[29] J. Song, C. Chen, S. Zhu, M. Zhu, J. Dai, U. Ray, Y. Li, Y. Kuang, Y. Li, N. Quispe, Y. Yao, A. Gong, U. H. Leiste, H. A. Bruck, J. Y. Zhu, A. Vellore, H. Li, M. L. Minus, Z. Jia, A. Martini, T. Li, L. Hu, *Nature* **2018**, *554*, 224.

[30] a) M. Antonietti, N. Fechler, T. P. Fellinger, *Chem. Mater.* **2014**, *26*, 196; b) S. Nardecchia, D. Carriazo, M. L. Ferrer, M. C. Gutierrez, F. del Monte, *Chem. Soc. Rev.* **2013**, *42*, 794; c) J. Biener, M. Stadermann, M. Suss, M. A. Worsley, M. M. Biener, K. A. Rose, T. F. Baumann, *Energy Environ. Sci.* **2011**, *4*, 656.

[31] C. Chen, J. Song, S. Zhu, Y. Li, Y. Kuang, J. Wan, D. Kirsch, L. Xu, Y. Wang, T. Gao, Y. Wang, H. Huang, W. Gan, A. Gong, T. Li, J. Xie, L. Hu, *Chem* **2018**, *4*, 544.

[32] S. C. Li, B. C. Hu, Y. W. Ding, H. W. Liang, C. Li, Z. Y. Yu, Z. Y. Wu, W. S. Chen, S. H. Yu, *Angew. Chem., Int. Ed.* **2018**, *57*, 7085.

[33] a) P. Sharma, T. S. Bhatti, *Energy Convers. Manage.* **2010**, *51*, 2901; b) J. Li, N. Wang, J. Tian, W. Qian, W. Chu, *Adv. Funct. Mater.* **2018**, *28*, 1806153; c) P. Simon, Y. Gogotsi, *Nat. Mater.* **2008**, *7*, 845.

[34] C. Chen, Y. Zhang, Y. Li, J. Dai, J. Song, Y. Yao, Y. Gong, I. Kierzewski, J. Xie, L. Hu, *Energy Environ. Sci.* **2017**, *10*, 538.

[35] Y. Wang, X. Lin, T. Liu, H. Chen, S. Chen, Z. Jiang, J. Liu, J. Huang, M. Liu, *Adv. Funct. Mater.* **2018**, *28*, 1806207.
[36] a) S. Teng, G. Siegel, W. Wang, A. Tiwari, *ECS Solid State Lett.* **2014**, *3*, M25; b) A. Cuña, N. Tancredi, J. Bussi, V. Barranco, T. A. Centeno, A. Quevedo, J. M. Rojo, *J. Electrochem. Soc.* **2014**, *161*, A1806; c) M.-C. Liu, L.-B. Kong, P. Zhang, Y.-C. Luo, L. Kang, *Electrochim. Acta* **2012**, *60*, 443.
[37] J. Jiang, L. Zhang, X. Wang, N. Holm, K. Rajagopalan, F. Chen, S. Ma, *Electrochim. Acta* **2013**, *113*, 481.
[38] L. Wei, M. Sevilla, A. B. Fuertes, R. Mokaya, G. Yushin, *Adv. Energy Mater.* **2011**, *1*, 870.
[39] Z. Tang, Z. Pei, Z. Wang, H. Li, J. Zeng, Z. Ruan, Y. Huang, M. Zhu, Q. Xue, J. Yu, C. Zhi, *Carbon* **2018**, *130*, 532.
[40] a) K. Qin, J. Kang, J. Li, E. Liu, C. Shi, Z. Zhang, X. Zhang, N. Zhao, *Nano Energy* **2016**, *24*, 158; b) P. Wu, S. Cheng, M. Yao, L. Yang, Y. Zhu, P. Liu, O. Xing, J. Zhou, M. Wang, H. Luo, *Adv. Funct. Mater.* **2017**, *27*, 1702160; c) Q. Qu, S. Yang, X. Feng, *Adv. Mater.* **2011**, *23*, 5574; d) J. Zhao, J. Chen, S. Xu, M. Shao, Q. Zhang, F. Wei, J. Ma, M. Wei, D. G. Evans, X. Duan, *Adv. Funct. Mater.* **2014**, *24*, 2938; e) F. Xin, Y. Jia, J. Sun, L. Dang, Z. Liu, Z. Lei, *ACS Appl. Mater. Interfaces* **2018**, *10*, 32192.
[41] A. Gutierrez-Pardo, B. Lacroix, J. Martinez-Fernandez, J. Ramirez-Rico, *ACS Appl. Mater. Interfaces* **2016**, *8*, 30890.
[42] M. Liu, M. Xu, Y. Xue, W. Ni, S. Huo, L. Wu, Z. Yang, Y.-M. Yan, *ACS Appl. Mater. Interfaces* **2018**, *10*, 31260.
[43] Y. Zhang, L. Zhang, K. Cui, S. Ge; X. Cheng, M. Yan, J. Yu, H. Liu, *Adv. Mater.* **2018**, *30*, 1801588.
[44] J. Edberg, O. Inganas, I. Engquist, M. Berggren, *J. Mater. Chem. A* **2018**, *6*, 145.
[45] C. Jia, T. Li, C. Chen, J. Dai, I. M. Kierzewski, J. Song, Y. Li, C. Yang, C. Wang, L. Hu, *Nano Energy* **2017**, *36*, 366.
[46] a) S.-Y. Chung, J. T. Bloking, Y.-M. Chiang, *Nat. Mater.* **2002**, *1*, 123; b) C. Liu, F. Li, L.-P. Ma, H.-M. Cheng, *Adv. Mater.* **2010**, *22*, E28; c) B. Scrosati, J. Hassoum, Y.-K. Sun, *Energy Environ. Sci.* **2011**, *4*, 3287.
[47] C. Chen, Y. Zhang, Y. Li, Y. Kuang, J. Song, W. Luo, Y. Wang, Y. Yao, G. Pastel, J. Xie, L. Hu, *Adv. Energy Mater.* **2017**. *7*, 1700595.
[48] a) T. Liu, R. Luo, W. Qiao, S.-H. Yoon, I. Mochida, *Electrochim. Acta* **2010**, *55*, 1696; b) T. Liu, R. Luo, S.-H. Yoon, I. Mochida, *Mater. Lett.* **2010**, *64*, 74.
[49] Y.-J. Han, D. Chung, K. Nakabayashi, J.-D. Chung, J. Miyawaki, S.-H. Yoon, *Electrochim. Acta* **2016**, *213*, 432.
[50] R. A. Adams, A. D. Dysart, R. Esparza, S. Acuña, S. R. Joshi, A. Cox, D. Mulqueen, V. G. Pol, *Ind. Eng. Chem. Res.* **2016**, *55*, 8706.
[51] Y. Zhang, W. Luo, C. Wang, Y. Li, C. Chen, J. Song, J. Dai, E. M. Hitz, S. Xu, C. Yang, Y. Wang, L. Hu, *Proc. Natl. Acad. Sci. USA* **2017**, *114*, 3584.
[52] C. Yang, Q. Gao, W. Tian, Y. Tan, T. Zhang, K. Yang, L. Zhu, *J. Mater. Chem. A* **2014**, *2*, 19975.
[53] Y. Li, H. Zhu, F. Shen, J. Wan, X. Han, J. Dai, H. Dai, L. Hu, *Adv. Funct. Mater.* **2014**, *24*, 7366.
[54] X. Liu, K. Wang, J. Chen, *Energy Storage Mater.* **2016**, *3*, 1.
[55] G. Liu, Y. Li, B. Wang, *Mater. Lett.* **2015**, *139*, 385.
[56] H. Zheng, J. Li, X. Song, G. Liu, V. S. Battaglia, *Electrochim. Acta* **2012**, *71*, 258.
[57] L. L. Lu, Y. Y. Lu, Z. J. Xiao, T. W. Zhang, F. Zhou, T. Ma, Y. Ni, H. B. Yao, S. H. Yu, Y. Cui, *Adv. Mater.* **2018**, *30*, 1706745.
[58] A. Manthiram, S. H. Chung, C. Zu, *Adv. Mater.* **2015**, *27*, 1980.
[59] D. Su, D. Zhou, C. Wang, G. Wang, *Adv. Funct. Mater.* **2018**, *28*, 1870273.
[60] M. Adam, P. Strubel, L. Borchardt, H. Althues, S. Dörfler, S. Kaskel, *J. Mater. Chem. A* **2015**, *3*, 24103.
[61] C. Schneidermann, C. Kensy, P. Otto, S. Oswald, L. Giebeler, D. Leistenschneider, S. Gratz, S. Dorfler, S. Kaskel, L. Borchardt, *ChemSusChem* **2019**, *12*, 310.
[62] Y. Li, K. K. Fu, C. Chen, W. Luo, T. Gao, S. Xu, J. Dai, G. Pastel, Y. Wang, B. Liu, J. Song, Y. Chen, C. Yang, L. Hu, *ACS Nano* **2017**, *11*, 4801.
[63] C. Luo, H. Zhu, W. Luo, F. Shen, X. Fan, J. Dai, Y. Liang, C. Wang, L. Hu, *ACS Appl. Mater. Interfaces* **2017**, *9*, 14801.
[64] Q. Pang, J. Tang, H. Huang, X. Liang, C. Hart, K. C. Tam, L. F. Nazar, *Adv. Mater.* **2015**, *27*, 6021.
[65] a) M. Balaish, J. Jung, II-D. Kim, Y. Ein-Eli, *Adv. Funct. Mater.* **2019**, 1808303; b) S. Chu, Y. Cui, N. Liu, *Nat. Mater.* **2017**, *16*, 16; c) J. Lu, L. Li, J. Park, Y. Sun, F. Wu, K. Amine, *Chem. Rev.* **2014**, *114*, 5611; d) X. Y. Luo, J. Lu, E. Sohm, L. Ma, T. P. Wu, J. G. Wen, D. T. Qiu, Y. K. Xu, Y. Ren, D. J. Miller, *Nano Res.* **2016**, *9*, 1913.
[66] a) Q. T. Liu, D. Liu, Z. Li, X. Zhang, Y. Zhang, *Adv. Mater.* **2016**, *28*, 8413; b) J. Zhang, Z. Xia, L. Dai, *Sci. Adv.* **2015**, *1*, e1500564; c) T. Liu, M. Leskes, W. Yu, A. J. Moore, L. Zhou, P. M. Bayley, G. Kim, C. P. Grey, *Science* **2015**, *350*, 530; d) Y. Cui, Z. Wen, Y. Liu, *Energy Environ. Sci.* **2011**, *4*, 4727; e) X. B. Zhu, T. S. Zhao, Z. H. Wei, P. Tan, L. An, *Energy Environ. Sci.* **2015**, *8*, 3745.
[67] J. Luo, X. Yao, L. Yang, Y. Han, L. Chen, X. Geng, V. Vattipalli, Q. Dong, W. Fan, D. Wang, H. Zhu, *Nano Res.* **2017**, *10*, 4318.
[68] H. Song, S. Xu, Y. Li, J. Dai, A. Gong, M. Zhu, C. Zhu, C. Chen, Y. Chen, Y. Yao, B. Liu, J. Song, G. Pastel, L. Hu, *Adv. Energy Mater.* **2018**, *8*, 1701203.
[69] C. Zhu, L. Du, J. Luo, H. Tang, Z. Cui, H. Song, S. Liao, *J. Mater. Chem. A* **2018**, *6*, 14291.
[70] C. Chen, S. Xu, Y. Kuang, W. Gan, J. Song, G. Chen, G. Pastel, B. Liu, Y. Li, H. Huang, L. Hu, *Adv. Energy Mater.* **2019**, *9*, 1802964.
[71] S. Xu, S. K. Das, L. A. Archer, *RSC Adv.* **2013**, *3*, 6656.
[72] S. Xu, C. Chen, Y. Kuang, J. Song, W. Gan, B. Liu, E. M. Hitz, J. W. Connell, Y. Lin, L. Hu, *Energy Environ. Sci.* **2018**, *11*, 3231.
[73] a) Y. Liu, C. Yang, Q. Zhang, M. Liu, *Energy Storage Mater.* **2019**, https://doi.org/10.1016/j.ensm.2019.01.001; b) H. L. Pan, Y. S. Hu, L. Q. Chen, *Energy Environ. Sci.* **2013**, *6*, 2338; c) X. Zheng, C. Bommier, W. Luo, L. Jiang, Y. Hao, Y. Huang, *Energy Storage Mater.* **2019**, *16*, 6.
[74] W. Luo, J. Schardt, C. Bommier, B. Wang, J. Razink, J. Simonsen, X. Ji, *J. Mater. Chem. A* **2013**, *1*, 10662.
[75] H. Zhu, Z. Jia, Y. Chen, N. Weadock, J. Wan, O. Vaaland, X. Han, T. Li, L. Hu, *Nano Lett.* **2013**, *13*, 3093.
[76] H. Zhu, F. Shen, W. Luo, S. Zhu, M. Zhao, B. Natarajan, J. Dai, L. Zhou, X. Ji, R. S. Yassar, *Nano Energy* **2017**, *33*, 37.
[77] F. Shen, W. Luo, J. Dai, Y. Yao, M. Zhu, E. Hitz, Y. Tang, Y. Chen, V. L. Sprenkle, X. Li, L. Hu, *Adv. Energy Mater.* **2016**, *6*, 1600377.
[78] Y. Zheng, Y. Lu, X. Qi, Y. Wang, L. Mu, Y. Li, Q. Ma, J. Li, Y.-S. Hu, *Energy Storage Mater.* **2019**, *18*, 269.
[79] X. Peng, L. Zhang, Z. Chen, L. Zhong, D. Zhao, X. Chi, X. Zhao, L. Li, X. Lu, K. Leng, C. Liu, W. Liu, W. Tang, K. P. Loh, *Adv. Mater.* **2019**, *31*, 1900341.